

ARMY RESEARCH LABORATORY



The Role of Wind Gusts in the Near-Ground Atmosphere

D. Keith Wilson

ARL-TR-2290

December 2000

Approved for public release; distribution unlimited.

20010223 105

The findings in this report are not to be construed as an official Department of the Army position unless so designated by other authorized documents.

Citation of manufacturer's or trade names does not constitute an official endorsement or approval of the use thereof.

Destroy this report when it is no longer needed. Do not return it to the originator.

Army Research Laboratory

Adelphi, MD 20783-1197

ARL-TR-2290

December 2000

The Role of Wind Gusts in the Near-Ground Atmosphere

D. Keith Wilson

Computational and Information Sciences Directorate

Approved for public release; distribution unlimited.

Abstract

Gusts from boundary-layer-scale convective eddies modify the structure of the atmospheric surface layer by intermittently intensifying or diminishing the local wind speed. A simple model for the effects of these gusts is proposed, based on the following two assumptions: (1) the wind gusts have an isotropic Gaussian probability distribution with standard deviation proportional to w_* (the convective velocity scale) and (2) the surface-layer wind and temperature profiles attain local equilibrium with the wind gusts. The minimum friction velocity predicted by the model has the same dependence on surface roughness predicted by Schumann's earlier "slab" model for convective boundary layers. However, the current model also applies to situations where the mean wind is nonzero. It predicts the breakdown of global Monin-Obukhov similarity for the surface-layer wind shear and temperature gradient in highly convective conditions (U_r/w_* approximately 1 or smaller, where U_r is the mean wind speed at the top of the surface layer). Also in contrast to existing similarity theories, the horizontal wind variance exhibits a significant dependence on height and surface roughness near the ground, even for moderate convection. The temperature variance is nearly unaffected by the gusts, because of its weak dependence on the local wind speed in convective conditions.

Contents

1	Introduction	1
2	Modeling Surface-Layer Gusts	3
2.1	Concept	3
2.2	Statistical Distribution	5
2.3	Nondimensionalization	9
2.4	Generalized Similarity Theory	12
3	Effect of Gusts on Atmospheric Statistics	15
3.1	Friction Velocity	15
3.2	Mean Profiles	18
3.3	Temperature Variance	23
3.4	Vertical Velocity Variance	25
3.5	Horizontal Velocity Variance	27
4	Summary	35
	Acknowledgments	36
	Appendices	37
A	Reference Height and Gustiness Coefficient	37
B	Moments of Friction Velocity and Wind Direction	39
	References	45
	Distribution	49
	Report Documentation Page	51

Figures

1	Vertical profiles of wind and temperature measured at different hypothetical stations, separated in either space or time . . .	4
2	Local wind speed as a function of local friction velocity	9
3	Global and average local friction velocity as a function of vector-average wind speed at reference height, U_r	16
4	Local average friction velocity as a function of roughness length for vanishing mean wind	18
5	Nondimensional wind gradient $(z\kappa/u_*)(d\langle U \rangle/dz)$ as a function of $\zeta = -z/L$	19
6	Nondimensional temperature gradient $(-z\kappa u_*/P_t Q_s)(d\langle T \rangle/dz)$ as a function of $\zeta = -z/L$	19
7	Ratio of friction velocity determined by fitting measurements at 10-m height to actual value determined from local-equilibrium model	21
8	Relative error (in %) between wind speed profile in local-equilibrium model and a profile determined by fitting u_* and T_* to measurements at 10-m height	22
9	Same as figure 8, except for temperature profile	22
10	Temperature variance predictions for $U_r/w_* = 0.3$	25
11	Ratio of vertical velocity variance (σ_u^2) predicted by local-equilibrium model to global similarity prediction, for a smooth surface ($z_0/z_i = 10^{-5}$)	26
12	Same as figure 11, but for a rough surface ($z_0/z_i = 10^{-3}$)	26
13	Comparison of approximate formula, equation (77), to local-equilibrium model prediction	28
14	Ratio of along-wind velocity variance (σ_u^2) predicted by local-equilibrium model to global similarity formula $0.45 w_*^2 + 5.8 u_*^2$, for a smooth surface ($z_0/z_i = 10^{-5}$)	31
15	Same as figure 14, but for a rough surface ($z_0/z_i = 10^{-3}$)	31
16	Ratio of along-wind to crosswind velocity variance (σ_u^2/σ_v) in local-equilibrium model, as a function of height, for a smooth surface ($z_0/z_i = 10^{-5}$)	32
17	Ratio of along-wind to crosswind velocity variance (σ_u^2/σ_v) in local-equilibrium model, smooth surface case ($z_0/z_i = 10^{-5}$)	32
18	Local equilibrium predictions for along-wind velocity variance using several methods of calculation	34
B-1	Statistical moments $\langle \bar{u}_{*L} \rangle$ and $\langle \bar{u}_{*L} \cos \theta \rangle$ as a function of normalized wind speed \bar{U}_r	43

B-2	Same as figure B-1, except for statistical moments $\langle \bar{u}_{*L} \cos^2 \theta \rangle$ and $\langle \bar{u}_{*L}^2 \cos^2 \theta \rangle$	43
-----	---	----

1. Introduction

One of the primary goals of micrometeorology is to develop statistical descriptions for the surface-layer (near-ground) structure of the atmosphere. These statistical descriptions have many valuable applications, such as forecasting the turbulent transport of biological and chemical agents and calculating the propagation of acoustic and electromagnetic waves. The most successful model for surface-layer statistics is the turbulence similarity theory developed by Monin and Obukhov (1954), which hypothesizes that the statistics depend on just four parameters: the friction velocity u_* , the surface temperature flux Q_s , the buoyancy coefficient $b = g/T_s$ (where g is gravitational acceleration and T_s , the surface temperature), and the height from the ground z . Note that no parameters in the Monin-Obukhov similarity theory are related to the large-scale structure of the atmospheric boundary layer.* The theory assumes that surface-layer processes are not significantly affected by the large boundary-layer-scale eddies (also called *thermals* or *plumes*) characteristic of convective conditions.†

Primarily during the 1960s and 1970s, semiempirical equations for the vertical profiles of mean wind and temperature were developed on the basis of Monin-Obukhov similarity. These equations fit the vertical profiles quite well and have since come into widespread use. Other statistics, such as the temperature and vertical velocity, have also been found to agree with the theory. Nonetheless, experiments have clearly demonstrated that not all near-ground statistics obey Monin-Obukhov similarity. Most significantly, the theory does not work well for the variance and spectrum of the horizontal wind components, which have been found to depend on z_i , the height of the boundary-layer capping temperature inversion (Kaimal et al, 1976; Caughey and Palmer, 1979; Khanna and Brasseur, 1997). Furthermore, Beljaars (1994) and Grachev et al (1998) demonstrated that parameterizations for surface fluxes and drag coefficients in convective conditions agree better with observations when the wind speed is replaced by a scalar average proportional to the mixed-layer velocity scale, $w_* = (Q_s z_i g / T_s)^{1/3}$, which is representative of the large eddies.

Potential limitations of Monin-Obukhov similarity in convective conditions were actually anticipated decades ago, apparently first by Businger

*The boundary layer is defined as "the layer of air directly above the Earth's surface in which the effects of the surface (friction, heating, and cooling) are felt directly on time scales less than a day" (Garratt, 1992, p. 1). It is typically 500 to 3000 m deep during the daytime. The surface layer can be thought of as the lowermost tenth of the atmospheric boundary layer.

†*Convective conditions* here means that boundary-layer turbulence is being produced primarily by buoyant instabilities, as opposed to wind shear. The buoyant instabilities usually dominate when there is solar heating of the ground.

(1973a,b). The main purposes of this report are to systematically address the behavior of surface-layer statistics in convective conditions and to provide a quantitative assessment of the breakdown of Monin-Obukhov similarity in these conditions. The framework I adopt is an extension of concepts developed by several previous authors, including Schumann (1988), Sykes et al (1993), Beljaars (1994), and Grachev et al (1997, 1998). The underlying principle is that large-scale convective eddies (circulations), which span the depth of the boundary layer, affect near-surface transfer processes by inducing a fluctuating local surface stress. Grachev et al (1997) aptly call this the *convection-induced stress regime* to differentiate it from the situation where stress is induced primarily by a steady wind. To quote those authors:

Close to the surface, a large-scale convective eddy has an instantaneous local wind profile which rapidly achieves a steady state. The local structure of such a profile should be essentially the same as in the usual mean wind profile (Kraichnan, 1962; Businger, 1973a). As a result, free convection can be treated as a particular case of forced convection (Sykes et al, 1993; Beljaars, 1994).

Therefore it is reasonable to apply the Monin-Obukhov similarity theory *locally* to statistics in the near-surface region of the large-scale convective eddies, even though application to *global* (ensemble) average statistics may be tenuous.

In section 2, I show how the premise of local equilibrium, when combined with a probability distribution for the wind gusts induced by the large-scale eddies, leads to a simple and workable methodology for calculating surface-layer statistics. This model is applied to the calculation of mean vertical profiles and variances in section 3. Two appendices follow the body of the report: appendix A discusses the value of numerical constants used in the model, and appendix B provides approximate analytical results for large-scale eddy effects on atmospheric statistics.

2. Modeling Surface-Layer Gusts

2.1 Concept

In the conventional decomposition of turbulence first proposed by Reynolds, fields such as wind and temperature are written as the sum of mean and fluctuating parts. For the wind velocity component aligned with the mean flow direction, the Reynolds decomposition is

$$U = \langle U \rangle + u, \quad (1)$$

where U is the instantaneous wind speed, u the fluctuation, and angle brackets indicate the ensemble mean. If we hypothesize that the turbulence attains a local equilibrium with the large-scale convective eddies, an appropriate alternative decomposition would be

$$U = \langle U \rangle_L + u, \quad (2)$$

where the subscript L on the angle brackets indicates a *local* mean value. The meaning of local here is admittedly imprecise. The general idea is that a spatial filter is applied in the horizontal plane, eliminating motions with scales smaller than those of the large-scale convective eddies. A filter having a cutoff in the range $0.1z_i$ to $0.3z_i$ would serve the desired purpose.* A filter in time could serve in place of the spatial one.

Since $\langle u \rangle$ is zero by hypothesis, if we take the global average (ensemble mean) of equation (2), it follows that the global average of locally averaged quantities is simply the global average:

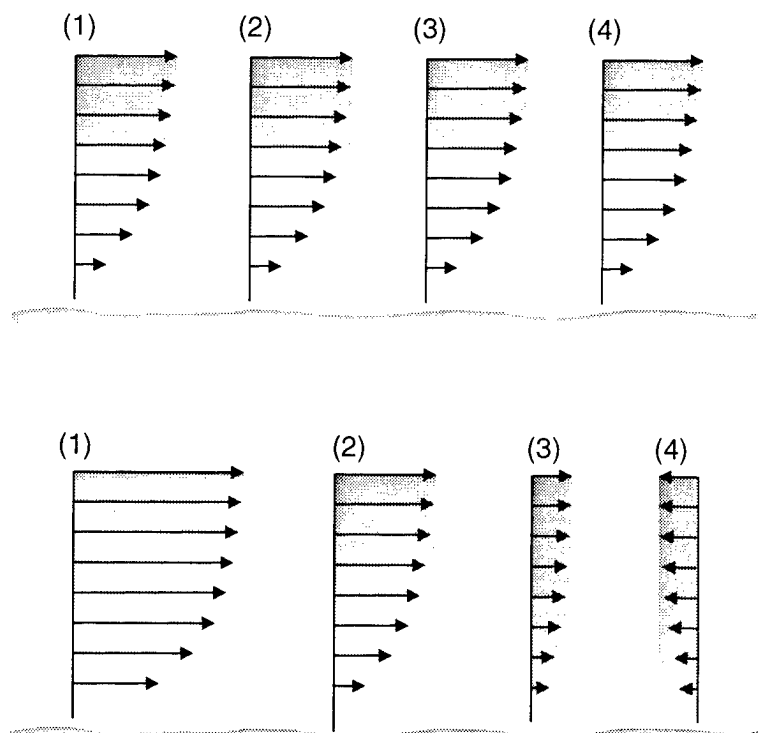
$$\langle U \rangle = \langle \langle U \rangle_L \rangle. \quad (3)$$

Throughout the rest of this report I refer to the variations in wind velocity resulting from large-scale convective eddies simply as *gusts*. This terminology is borrowed from previous authors, including Godfrey and Beljaars (1991) and Grachev et al (1998). Colloquially, "gusts" can refer to variations in the wind velocity other than those originating from large-scale convective eddies, such as activity associated with a thunderstorm or a frontal passage.

Figure 1 illustrates the concept that local vertical profiles of wind and temperature obtain equilibrium with gusts, as opposed to the actual mean

*The concept of applying a filter to separate large-scale motions from smaller ones is discussed in more detail by Tong et al (1998). The purpose of the filter in this report is to separate the large-scale convective eddies from other smaller scale motions. The purpose of Tong et al was somewhat different: to mimic the resolvable-/subgrid-scale partition in large-eddy simulation.

Figure 1. Vertical profiles of wind and temperature measured at different hypothetical stations (1-4), separated in either space or time. Profiles are averaged with local filter. Upper: Profiles for a flow having no significant gustiness. Lower: Profiles for a flow having pronounced gustiness. Local temperature profiles are in equilibrium with gusts. (Arrows represent horizontal wind velocity. Gray scale represents temperature, with light shading being warmer air.)



wind, $\langle U \rangle$. Shown in the figure are the vertical profiles of wind and temperature, after applying the local filter $\langle \rangle_L$, at different measurement locations. For the hypothetical situation illustrated in the upper part of the figure, the flow structure at scales greater than the filter cutoff is negligible, so all the observed local profiles are nearly identical. The wind speed increases roughly logarithmically with height, and a layer of warm air lies next to the ground. The local profiles at each station are in equilibrium with the mean wind speed. For the situation illustrated in the lower part of the figure, gusting is significant, and the local wind and temperature profiles come into equilibrium with the gusts. At station (1), a locally strong gust is mixing warm air upward from the ground. At station (2), little deviation of $\langle U \rangle_L$ from $\langle U \rangle$ occurs so that the wind and temperature profiles are the same as in the upper figure. At station (3), motion from a large-scale eddy is in the opposite direction of the prevailing wind, hence decreasing the local wind speed. As a result, turbulent mixing is weakened, and most of the warm air remains near the ground. If the motion from a large-scale eddy is strong enough, the wind may actually shift direction from the prevailing one, as shown for station (4).

Strictly speaking, neither of the situations illustrated in figure 1 pertains to the customary application of Monin-Obukhov similarity theory; that theory applies to the ensemble flow characteristics. Even though the wind may vary locally because of individual gusts, the flow is *not* required to obtain a local equilibrium with them. Local states of the flow are just samples of the global ensemble, and the similarity theory is intended only for the global ensemble. However, one might anticipate that Monin-Obukhov similarity

cannot be applied satisfactorily to a global ensemble *unless* the local flow samples are all nearly the same as the global average, as in the upper part of figure 1. Otherwise, the premise that large- (z_i -) scale eddies do not significantly affect the near-ground flow is violated.

What justification does one have, though, for applying Monin-Obukhov similarity to locally averaged flow fields? A simple supportive argument follows from the relative time scales of the large-scale convective eddies and the smaller surface-layer ones. The convective eddies have a time scale of z_i/w_* . Taking $z_i \sim 1000$ m and $w_* \sim 2$ m/s as representative implies an approximate time scale of about 8 min. The surface-layer eddies have a time scale of z/u_* ; with $z \sim 10$ m and $u_* \sim 0.3$ m/s, z/u_* is about 30 s. Therefore the time scale of the convective eddies should be one to two orders of magnitude larger than that of the surface-layer eddies. Given this disparity, one might reasonably expect the surface-layer eddies to obtain a rough equilibrium with the gusts.

So far, I have discussed only large-scale variations in wind velocity. Of course other quantities, such as the surface heat flux or temperature, could also vary locally. These variations could even occur over uniform terrain, as a result of clouds blocking incoming solar radiation, and other processes. In this report I chose to neglect such possible variations for simplicity, although these could be treated in a manner analogous to the wind gusts.

2.2 Statistical Distribution

This section builds a general framework for calculating modifications to surface-layer statistics caused by the gusts (large-scale convective eddies). The basic idea is to specify a probability density function for the wind-velocity components at some reference height. Local application of Monin-Obukhov similarity then allows calculation of other statistics.

To begin, we follow Godfrey and Beljaars (1991) and Grachev et al (1998) by defining a horizontal gust velocity \mathbf{G} (the contribution of the large-scale convective eddies to the local wind, denoted W_G by Godfrey and Beljaars and \tilde{U} by Grachev et al) through the relation

$$\mathbf{U}_L(z) = \langle \mathbf{U}(z) \rangle + \mathbf{G}(z) . \quad (4)$$

(Boldface type in this report indicates a vector quantity; the same symbol without bolding represents the magnitude of the vector.) Taking the squared magnitude of both sides of equation (4) results in

$$U_L^2(z) = [\langle U(z) \rangle + G_x(z)]^2 + G_y^2(z) , \quad (5)$$

where $G_x(z)$ and $G_y(z)$ are the along-wind and crosswind components of the gust velocity, respectively. Averaging both sides, while keeping in mind that $\langle \mathbf{G}(z) \rangle = 0$, results in

$$\langle U_L^2(z) \rangle = \langle U(z) \rangle^2 + \langle G^2(z) \rangle , \quad (6)$$

where $\langle G^2(z) \rangle = \langle G_x^2(z) \rangle + \langle G_y^2(z) \rangle$. Godfrey and Beljaars and Grachev et al set

$$\langle G^2(z_r) \rangle = \beta^2 w_*^2. \quad (7)$$

where β is an empirical factor, called the *gustiness coefficient*. In this report, I set $\beta = 0.95$ and $z_r = 0.1 z_i$ for reasons discussed in appendix A. For brevity, I usually drop the explicit functional dependence of quantities such as $U(z)$ and $G(z)$ on z when they are to be evaluated at $z = z_r$. I also abbreviate the local wind velocity $\langle U(z_r) \rangle_L$ as U_L , and $\langle U(z_r) \rangle$ as U_r .

Provided that the gusts have random orientation, equation (7) implies that the variances $\langle G_x^2 \rangle$ and $\langle G_y^2 \rangle$ at the reference height must individually be $\beta^2 w_*^2 / 2$. To complete a probabilistic model, I will make the assumption that G_x and G_y are independent, Gaussian random variables. The approximate Gaussian nature of turbulent fluctuations is well established (Batchelor, 1953, pp 169–170), whereas the independence of G_x and G_y follows from the isotropic nature of the gusts. The joint probability density function (pdf) for G_x and G_y is therefore

$$p_G(G_x, G_y) = \frac{1}{\pi \beta^2 w_*^2} \exp \left(-\frac{G_x^2 + G_y^2}{\beta^2 w_*^2} \right). \quad (8)$$

Given the pdf for the gusts, surface-layer statistics can be calculated from the general formula

$$\langle f(U_r, Q_s, z, z_0, z_i, g/T_s) \rangle = \int_{-\infty}^{\infty} \int_{-\infty}^{\infty} f(U_r, Q_s, z, z_0, z_i, g/T_s, G_x, G_y) p_G(G_x, G_y) dG_x dG_y, \quad (9)$$

where $f(U_r, Q_s, z, z_0, z_i, g/T_s, G_x, G_y)$ is a function of interest, and $\langle f(U_r, Q_s, z, z_0, z_i, \dots) \rangle$ its ensemble mean. As an example, consider the mean wind speed at the reference height, $\langle U_L \rangle$. Since

$$U_L(U_r, G_x, G_y) = \sqrt{(U_r + G_x)^2 + G_y^2}, \quad (10)$$

we have

$$\langle U_L \rangle = \frac{1}{\pi \beta^2 w_*^2} \int_{-\infty}^{\infty} \int_{-\infty}^{\infty} \sqrt{(U_r + G_x)^2 + G_y^2} \exp \left(-\frac{G_x^2 + G_y^2}{\beta^2 w_*^2} \right) dG_x dG_y. \quad (11)$$

Solution of this type of integral is discussed in appendix B. The result is

$$\frac{\langle U_L \rangle}{\beta w_*} = \frac{\sqrt{\pi}}{2} e^{-\bar{U}_r^2/2} \left[\left(1 + \bar{U}_r^2 \right) I_0 \left(\frac{\bar{U}_r^2}{2} \right) + \bar{U}_r^2 I_1 \left(\frac{\bar{U}_r^2}{2} \right) \right], \quad (12)$$

where $\bar{U}_r = U_r / \beta w_*$, and the I_n 's are modified Bessel functions of the first kind. In the limit $\bar{U}_r \rightarrow 0$, one can show $\langle U_L \rangle \rightarrow \sqrt{\pi} \beta w_* / 2$.

Of course, to be useful, this method must be extended to quantities in addition to $\langle U_L \rangle$. We would like to calculate, for example, mean profiles and variances in the presence of gusts. This is where the assumption of local equilibrium enters into the problem. The basic strategy is to use local equilibrium to determine a *local friction velocity*, u_{*L} , as a function of $(U_r, Q_s, z, z_0, z_i, g/T_s, G_x, G_y)$. Then, given an equation for the quantity of interest in terms of the friction velocity, we can apply equation (9) to determine its statistics.

The basic Monin-Obukhov similarity equations for the vertical gradients of mean wind and temperature are the starting point for formulating such a solution.* These are (e.g., Panofsky and Dutton, 1984; Kader and Yaglom, 1990)

$$\frac{d\langle U \rangle}{dz} = \frac{u_*}{\kappa z} \phi_M \left(\frac{z}{L} \right), \quad \text{and} \quad (13)$$

$$\frac{d\langle T \rangle}{dz} = \frac{P_t T_*}{\kappa z} \phi_H \left(\frac{z}{L} \right). \quad (14)$$

Here $T_* = -Q_s/u_*$ is the surface-layer temperature scale, $\kappa \simeq 0.40$ is the von Kármán constant, and $P_t \simeq 0.9$ is the turbulent Prandtl number. The functions ϕ_M and ϕ_H are hypothesized to have a universal dependence on the nondimensional height $\zeta = z/L$, where $L = -u_*^3 T_s / (\kappa g Q_s)$ is called the Obukhov length. The form I use in this report for the functions ϕ_M and ϕ_H is (Carl et al, 1973)

$$\phi_{M,H}(\zeta) = (1 - a_{M,H}\zeta)^{-1/3}, \quad (15)$$

where a_M and a_H are empirical constants. The vertical profiles, found by integrating equations (13) and (14), are

$$\langle U(z) \rangle = \frac{u_*}{\kappa} \left[\ln \frac{z}{z_0} - \Psi_M \left(\frac{z}{L} \right) + \Psi_M \left(\frac{z_0}{L} \right) \right], \quad \text{and} \quad (16)$$

$$\langle T(z) \rangle = T(z_h) + \frac{T_* P_t}{\kappa} \left[\ln \frac{z}{z_h} - \Psi_H \left(\frac{z}{L} \right) + \Psi_H \left(\frac{z_h}{L} \right) \right]. \quad (17)$$

The quantity z_0 is the aerodynamic roughness length (the height at which the velocity vanishes), and z_h is a reference height where the temperature is measured. The functions Ψ_M and Ψ_H are defined by

$$\Psi_{M,H}(\xi) \equiv \int_0^\xi \frac{1 - \phi_{M,H}(x)}{x} dx. \quad (18)$$

Performing this integration, one finds (Grachev et al, 1998)

$$\Psi_{M,H}(\xi) = \frac{3}{2} \ln \frac{1 + \phi_{M,H}^{-1} + \phi_{M,H}^{-2}}{3} - \sqrt{3} \arctan \frac{1 + 2\phi_{M,H}^{-1}}{\sqrt{3}} + \frac{\pi}{\sqrt{3}}. \quad (19)$$

*Throughout this report, I use "temperature" implicitly to mean the *virtual potential temperature*. The virtual potential temperature includes corrections for the effect of water vapor and air buoyancy (Stull, 1988).

The basic premise of the local equilibrium theory is that these equations apply locally to the gusts. Hence we replace them with

$$\langle \mathbf{U}(z) \rangle_L = (\mathbf{e}_x \cos \theta + \mathbf{e}_y \sin \theta) \frac{u_{*L}}{\kappa} \left[\ln \frac{z}{z_0} - \Psi_M \left(\frac{z}{L_L} \right) + \Psi_M \left(\frac{z_0}{L_L} \right) \right], \quad \text{and} \quad (20)$$

$$\langle T(z) \rangle_L = T(z_h) - \frac{P_t Q_s}{\kappa u_{*L}} \left[\ln \frac{z}{z_h} - \Psi_H \left(\frac{z}{L_L} \right) + \Psi_H \left(\frac{z_h}{L_L} \right) \right]. \quad (21)$$

where θ is the local wind direction, u_{*L} is the local friction velocity induced by the gusts, $L_L = u_{*L}^3 T_s / (\kappa g Q_s)$, and \mathbf{e}_x and \mathbf{e}_y are the unit vectors in the x - and y -directions. Orienting the coordinate system so that the mean wind direction is along the x -axis, one has immediately (with application of the constraint $\langle \mathbf{U} \rangle = \langle \langle \mathbf{U} \rangle_L \rangle$)

$$\left\langle u_{*L} \cos \theta h_M \left(\frac{z}{L_L}, \frac{z_0}{L_L} \right) \right\rangle = \kappa \langle U(z) \rangle, \quad \text{and} \quad (22)$$

$$\left\langle u_{*L} \sin \theta h_M \left(\frac{z}{L_L}, \frac{z_0}{L_L} \right) \right\rangle = 0, \quad (23)$$

where

$$h_{M,H}(x, y) = \ln \frac{x}{y} - \Psi_{M,H}(x) + \Psi_{M,H}(y). \quad (24)$$

Taking the magnitude of equation (20) results in

$$U_L = \frac{u_{*L}}{\kappa} h_M \left(\frac{z_r}{L_L}, \frac{z_0}{L_L} \right). \quad (25)$$

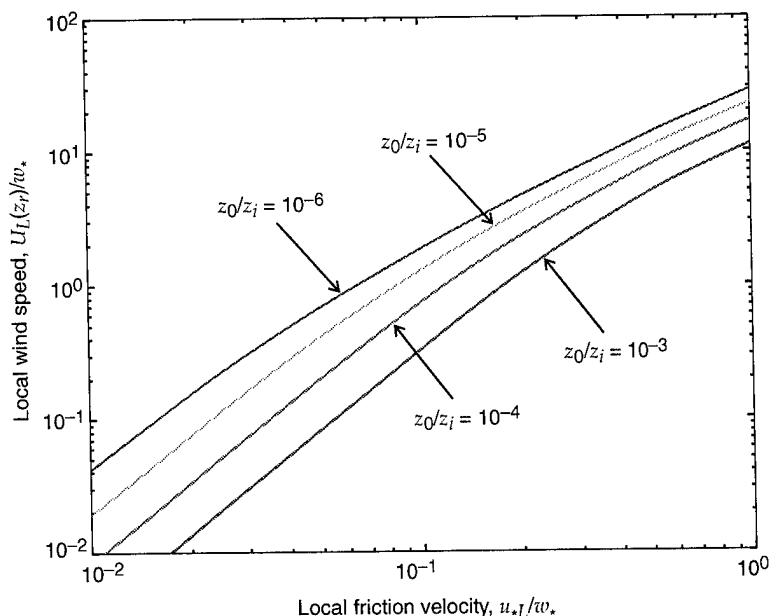
Equating this result to equation (10) yields

$$\sqrt{(U_r + G_x)^2 + G_y^2} = \frac{u_{*L}}{\kappa} h_M \left(\frac{z_r}{L_L}, \frac{z_0}{L_L} \right). \quad (26)$$

This equation can be solved, in principle, for u_{*L} as a function of U_r , Q_s , z_0 , z_i , g/T_s , G_x , and G_y . However because h_M in equation (25) is a complicated nonlinear function of L_L and L_L is in turn proportional to u_{*L}^3 , it is not possible to analytically solve equation (25) for u_{*L} . Fortunately the equation can be solved numerically for u_{*L} without difficulty. The simplest method is to calculate a look-up table of U_L values for a range of uniformly distributed u_{*L} values. Then, given a new value of U_L , the corresponding value of u_{*L} can be found by interpolating in the table. Figure 2 shows the dependence of U_L/w_* on u_{*L}/w_* for several values of z_0/z_i . (The motivation for normalizing the velocities by w_* and then plotting with z_0/z_i as a parameter are discussed in sect. 2.3.)

When temperature statistics are calculated, it is necessary to specify z_h and $T(z_h)$ in equation (21). This is actually very problematic in the context of the local equilibrium model. The most reasonable approach may initially seem to be setting z_h and $T(z_h)$ to constant (global) values, with $T(z_h)$

Figure 2. Local wind speed as a function of local friction velocity. Four curves are shown, corresponding to different values of ratio z_0/z_i . (For $z_i = 1000$ m, $z_0/z_i = 10^{-5}$ is representative of a grassy surface, whereas 10^{-4} is representative of mature crops or brush.)



being the surface temperature and z_h the thermal roughness length of the surface. The problem with this approach is that the local fluctuations in u_{*L} (and therefore T_{*L}) then create extremely large temperature fluctuations at $z = z_r$. These fluctuations are associated with turbulence length scales above the cutoff for the local filter; that is, they come from the convective, z_i -scale eddies whose velocity fluctuations are specified by equation (8). In actuality, observations suggest that the temperature variance σ_T^2 does not depend on the large eddies, even well above the surface layer. Therefore this approach is not physically realistic. The root of the difficulty is that z_h and $T(z_h)$ vary in response to the gusts. As discussed by Panofsky and Dutton (1984, p 147), z_h should be order k_h/u_* , where k_h is the molecular coefficient of heat conduction. In the context of local equilibrium, then, z_h is order k_h/u_{*L} . When the wind slackens, the layer adjacent to the ground thickens where molecular heat conduction dominates. A strong gust extends turbulent mixing closer to the surface, causing the molecular layer to shrink.

To circumvent the problem of specifying the dynamic response of z_h and $T(z_h)$ to gusts, I will assume that the variance of the locally averaged temperature fluctuations, $\langle T_G^2 \rangle$ (where $T_G = \langle T \rangle_L - \langle T \rangle$), is zero at $z = z_r$, as is consistent with observations. Then we can simply apply equation (21) with $z_h = z_r$ and with $T(z_r)$ fixed to the global value. Results derived from this approach must be viewed as speculative; fortunately only a few of the calculations (specifically the temperature gradient and variance) in this report depend on it.

2.3 Nondimensionalization

Suppose we apply the methodology in the previous section to determine statistics in the atmospheric surface layer. Such statistics would generally

depend on the parameters U_r , Q_s , g/T_s , z , z_0 , and z_i . (Other parameters, such as L and w_* , can be written as combinations of this set.) It would be rather clumsy, though, to systematically study the dependence of the statistics on all five of these parameters. Therefore we might ask whether the parameter dependence can be simplified in some fashion. In this section I show that it is possible to reduce the dependence to just three basic ratios involving the five original parameters, specifically U_r/w_* , z/z_i , and z_0/z_i . The z/z_i dependence drops out if z is not part of the original parameter set.

As will become apparent in section 3, most wind and temperature statistics of interest are proportional to ensemble averages involving powers of the local friction velocity, along with cosines and sines of the local wind direction. Therefore we are faced with the general problem of converting a function whose explicit dependence is on u_{*L} , $\cos \theta$, and $\sin \theta$, to one with dependence on U_r , Q_s , etc, so that equation (9) can be applied. To start, consider equation (25) evaluated at $z = z_r$ and recast in the following form:

$$\frac{U_L}{w_*} = \frac{1}{\kappa} \frac{u_{*L}}{w_*} h_M \left(-\frac{\kappa z_r u_*^3}{z_i u_{*L}^3}, -\frac{\kappa z_0 u_*^3}{z_i u_{*L}^3} \right). \quad (27)$$

This version uses the relationship $L_L = -(z_i/\kappa) (u_{*L}/w_*)^3$. Since the value $0.1 z_i$ is used for z_r , the right-hand side is a function entirely of u_{*L}/w_* and z_0/z_i . If I assume that h_M is an invertible function, then some function b must exist such that

$$\frac{u_{*L}}{w_*} = b \left(\frac{U_L}{w_*}, \frac{z_0}{z_i} \right) = b \left(\sqrt{\left(\frac{U_r}{w_*} + \frac{G_x}{w_*} \right)^2 + \left(\frac{G_y}{w_*} \right)^2}, \frac{z_0}{z_i} \right). \quad (28)$$

Furthermore, from basic trigonometric arguments,

$$\cos \theta = \frac{U_r + G_x}{\sqrt{(U_r + G_x)^2 + G_y^2}}, \quad \text{and} \quad (29)$$

$$\sin \theta = \frac{G_y}{\sqrt{(U_r + G_x)^2 + G_y^2}}. \quad (30)$$

With h_M given by equations (19) and (24), analytical determination of the function b is impossible. The important point here, though, is the existence of the function b . Now, suppose we wish to know the average value of some function $f(u_{*L}/w_*, \theta)$. Using equations (28), (29), and (30) to determine the dependence of f on U_r/w_* , G_x/w_* , G_y/w_* , and z_0/z_i results in the probability integral

$$\left\langle f \left(\frac{u_{*L}}{w_*}, \theta \right) \right\rangle = \int_{-\infty}^{\infty} \int_{-\infty}^{\infty} f \left[b \left(\sqrt{\left(\frac{U_r}{w_*} + \frac{G_x}{w_*} \right)^2 + \left(\frac{G_y}{w_*} \right)^2}, \frac{z_0}{z_i} \right), \arctan \left(\frac{G_y}{U_r + G_x} \right) \right] p_G(G_x, G_y) dG_x dG_y. \quad (31)$$

Transforming the variables of integration to the dimensionless ratios $G'_x = G_x/w_*$ and $G'_y = G_y/w_*$, and assuming that the joint pdf depends only on these ratios (as does the Gaussian pdf in the previous section, eq (8)), I have

$$\left\langle f\left(\frac{u_{*L}}{w_*}, \theta\right) \right\rangle = \int_{-\infty}^{\infty} \int_{-\infty}^{\infty} f \left[b \left(\sqrt{\left(\frac{U_r}{w_*} + G'_x\right)^2 + G'^2_y}, \frac{z_0}{z_i} \right), \arctan\left(\frac{G_y}{U_r + G_x}\right) \right] p_G(G'_x, G'_y) dG'_x dG'_y. \quad (32)$$

The function f now depends entirely on U_r/w_* , z_0/z_i , G'_x , and G'_y . The dependence of $\langle f \rangle$ on G'_x and G'_y is of course eliminated by the integration, leaving

$$\left\langle f\left(\frac{u_{*L}}{w_*}, \theta\right) \right\rangle = g\left(\frac{U_r}{w_*}, \frac{z_0}{z_i}\right), \quad (33)$$

where g is the result of the integration. This theorem demonstrates that statistics involving u_{*L}/w_* and/or θ depend only on U_r/w_* and z_0/z_i , although in practice it may be impossible to actually obtain an analytical expression for the function $g(U_r/w_*, z_0/z_i)$.

An interesting special case of the preceding theorem that applies to the average friction velocity in the limit of vanishing mean wind was proposed by Businger (1973b). He suggested that

$$\frac{\langle u_{*L} \rangle}{w_*} = g_B\left(\frac{z_i}{z_0}\right), \quad (34)$$

where g_B is an unknown function. The validity of this scaling relationship was later supported by Schumann's (1988) analysis based on a simplified bulk model for the atmospheric surface layer. Equation (33) implies the same scaling relationship, since the dependence on U_r/w_* disappears in the limit of vanishing U_r . In this report, the procedure for deriving this relationship was much different from Schumann's, however, being based instead on the statistical nature of the gusts. Furthermore, it is now clear that any statistic of u_{*L} and/or θ depends solely on z_0/z_i when the mean wind is zero.

Several valuable corollaries of equation (33) can be easily derived. First, let us consider statistics of quantities that additionally depend on z/L_L . Since $z/L_L \propto (z/z_i)(w_*/u_{*L})^3$ and the ratio w_*/u_{*L} has already been accounted for, a dependence on z/z_i is introduced:

$$\left\langle f\left(\frac{u_{*L}}{w_*}, \frac{z}{L_L}, \theta\right) \right\rangle = g\left(\frac{U_r}{w_*}, \frac{z}{z_i}, \frac{z_0}{z_i}\right). \quad (35)$$

A local dependence on z_0/L_L would not add new dependencies to the result, since $z_0/L_L \propto (z_0/z_i)(w_*/u_{*L})^3$. Next consider statistics that depend on $T_{*L} = -Q_s/u_{*L}$, as is usually the case for functions involving temperature. Defining a mixed-layer temperature scale as $\theta_* = -Q_s/w_*$, we can

write $T_{*L}/\theta_* = w_*/u_{*L}$. Again, no new dependencies are added to the result. Hence we have, most generally,

$$\left\langle f \left(\frac{u_{*L}}{w_*}, \frac{T_{*L}}{\theta_*}, \frac{z}{L_L}, \frac{z_0}{L_L}, \theta \right) \right\rangle = g \left(\frac{U_r}{w_*}, \frac{z}{z_i}, \frac{z_0}{z_i} \right). \quad (36)$$

An important application of equation (35) made later in this report is to statistics of the height-dependent gust profiles $G_x(z)$ and $G_y(z)$. From equations (20) and (4), we find

$$\frac{G_x(z)}{w_*} = \frac{1}{\kappa} \frac{u_{*L}}{w_*} \cos \theta h_M \left(\frac{z}{L_L}, -\frac{\kappa z_0 u_*^3}{z_i u_{*L}^3} \right) - \frac{\langle U(z) \rangle}{w_*}, \quad \text{and} \quad (37)$$

$$\frac{G_y(z)}{w_*} = \frac{1}{\kappa} \frac{u_{*L}}{w_*} \sin \theta h_M \left(\frac{z}{L_L}, -\frac{\kappa z_0 u_*^3}{z_i u_{*L}^3} \right). \quad (38)$$

The terms in equations (37) and (38) involving the function h_M depend on u_{*L}/w_* , z/L_L , and z_0/z_i . Therefore, equation (35) shows that statistics of these terms depend on U_r/w_* , z/z_i , and z_0/z_i . Taking the global average of equation (20) yields

$$\frac{\langle U(z) \rangle}{w_*} = \frac{1}{\kappa} \left\langle \frac{u_{*L}}{w_*} \cos \theta h_M \left(\frac{z}{L_L}, -\frac{\kappa z_0 u_*^3}{z_i u_{*L}^3} \right) \right\rangle. \quad (39)$$

We see that this term also depends on U_r/w_* , z/z_i , and z_0/z_i . Therefore

$$\left\langle f \left(\frac{G_x(z)}{w_*}, \frac{G_y(z)}{w_*} \right) \right\rangle = g \left(\frac{U_r}{w_*}, \frac{z}{z_i}, \frac{z_0}{z_i} \right). \quad (40)$$

2.4 Generalized Similarity Theory

Although it is not immediately obvious, the nondimensionalization theorems in the previous section imply modifications to the Monin-Obukhov and other similarity theories for the surface layer. Before discussing these modifications, I will review several of the common similarity theories:

Monin-Obukhov similarity (Monin and Obukhov, 1954): The basic physical parameters hypothesized to be significant are u_* , Q_s , $b = g/T_s$, and z . This parameter set possesses only three fundamental physical dimensions: length, time, and temperature. According to Buckingham's π theorem (see, for example, Stull, 1988), we should therefore select just three of these parameters as key. The three that are conventionally selected are u_* , Q_s , and z . Quantities scaled (made dimensionless) by these parameters must be functions of a single dimensionless ratio. This dimensionless ratio is taken to be z/L , where $L = -u_*^3 T_s / (\kappa g Q_s)$ is the Obukhov length. (The minus sign and constant κ in L are also matters of convention.)

Local free-convection similarity (Wyngaard et al, 1971): The basic physical parameters are the same as Monin-Obukhov similarity, except that u_* is dropped from the set. The remaining three parameters incorporate the

three physical dimensions of length, time, and temperature. As no dimensionless combinations can be formed from these parameters, quantities scaled by them must be constant. For example, quantities with dimensions of velocity, when divided by the derived scale $u_f = (Q_s z g / T_s)^{1/3}$, are constant.

Mixed-layer similarity (Deardorff, 1970): This scheme is the same as free-convection similarity, except that z_i replaces z . The velocity scale $w_* = (Q_s z_i g / T_s)^{1/3}$ therefore replaces u_f .

All three of the preceding similarity theories have been applied to surface-layer statistics. Monin-Obukhov similarity is widely applied to the mean profiles for both mechanical and convective turbulence. Local free-convection similarity is applied to the temperature and vertical velocity variance in convective conditions. Mixed-layer similarity is applied to the horizontal velocity variance in convective conditions.

Suppose now that the parameters from all three of these schemes are combined, resulting in the five-parameter set u_* , Q_s , b , z , and z_i . Three of these parameters (or combinations thereof) can be taken as key. Quantities scaled by the three key parameters must depend on two dimensionless ratios. Numerous combinations of key parameters and dimensionless ratios are possible. To generalize Monin-Obukhov similarity, we would logically take u_* , Q_s , and z as the key parameters, and the two dimensionless ratios as z/L and z_i/L . Alternatively, we could formulate a generalized mixed-layer scheme with Q_s , b , and z_i as the key parameters. For the dimensionless ratios, the only restriction is that u_* and z must be uniquely recoverable. So we may take these ratios to be u_*/w_* and z/z_i , for example.

The roughness length z_0 is not included in any of the three similarity theories described earlier. Omission of z_0 can be justified on the basis that the structure of a high Reynolds number flow should be independent of roughness at heights $z \gg z_0$ (Tennekes and Lumley, 1972, p 146). However, this reasoning overlooks possible interactions between large-scale eddies and the surface, a phenomenon that plays a central role in the model described in this report. Therefore z_0 should generally be included in the parameter set. Forming a six-parameter set by adding z_0 to the five discussed in the preceding paragraph, we conclude that scaled quantities must depend on three dimensionless ratios. For the generalized mixed-layer scheme, these can be taken to be u_*/w_* , z/z_i , and z_0/z_i .

The nondimensionalization theorems in section 2.3 are closely analogous to this generalized roughness-inclusive mixed-layer scheme. The main difference is that mean wind speed U_r appears in place of u_* . Such a scaling could have been argued by choosing U_r , Q_s , b , z , z_0 , and z_i as the initial six-parameter set, as long as the reference height does not introduce a new scale (i.e., the reference height must be proportional to either z_0 or z_i). The reason for preferring U_r over u_* in the present model is that it simplifies the formulation of the pdf for the wind velocity at the reference height. We now see that the nondimensionalization theorems are consistent with, and

could have been anticipated on the basis of, a generalized mixed-layer similarity theory that incorporates U_r , z , and z_0 , in addition to the standard parameters Q_s , z_i , and b . The model in section 2.2 provides a framework for calculating the similarity functions.

3. Effect of Gusts on Atmospheric Statistics

In this section, I apply the framework for calculating gust effects on atmospheric statistics. The calculations involve the numerical integration of equation (9) with $p_G(G_x, G_y)$ given by equation (8), and u_{*L} determined from equation (25). The numerical integrations were done on a square grid defined by $-12w_* \leq (G_x, G_y) \leq 12w_*$. The grid had 201 evenly spaced points in both the x - and y -directions. The calculations require only a few seconds each on a desktop personal computer.

3.1 Friction Velocity

Let us begin by applying the methodology developed in section 2.2 to the friction velocity. The familiar global version of the friction velocity u_* is defined through the equation

$$u_*^2 = -\langle uw \rangle . \quad (41)$$

In this equation, u is the fluctuation in the horizontal wind component aligned with the mean wind and w is the fluctuation in the vertical component. Similarly, the local friction velocity is defined as

$$u_{*L}^2 = -\langle u'w \rangle_L , \quad (42)$$

where the prime indicates the coordinate system aligned with the local wind direction θ . By elementary trigonometry,

$$u = u' \cos \theta - v' \sin \theta , \quad (43)$$

where v is the horizontal crosswind component of the wind. Multiplying through by $-w$ and taking the local average, one finds

$$-\langle uw \rangle_L = -\langle u'w \rangle_L \cos \theta + \langle v'w \rangle_L \sin \theta . \quad (44)$$

When I substitute equation (42) and set $\langle v'w \rangle_L = 0$ (a result of local symmetry in the turbulence statistics), this becomes

$$-\langle uw \rangle_L = u_{*L}^2 \cos \theta . \quad (45)$$

Now, by taking the global average and recalling that the global average of a local average equals the customary global average (see sect. 2.1), one obtains the result

$$u_*^2 = \langle u_{*L}^2 \cos \theta \rangle . \quad (46)$$

We see that the global friction velocity is not the simple average of the local one. The changing wind direction plays a role through the factor $\cos \theta$. If θ

is randomly distributed in all directions, the $\cos \theta$ factor has zero mean, and u_* vanishes.

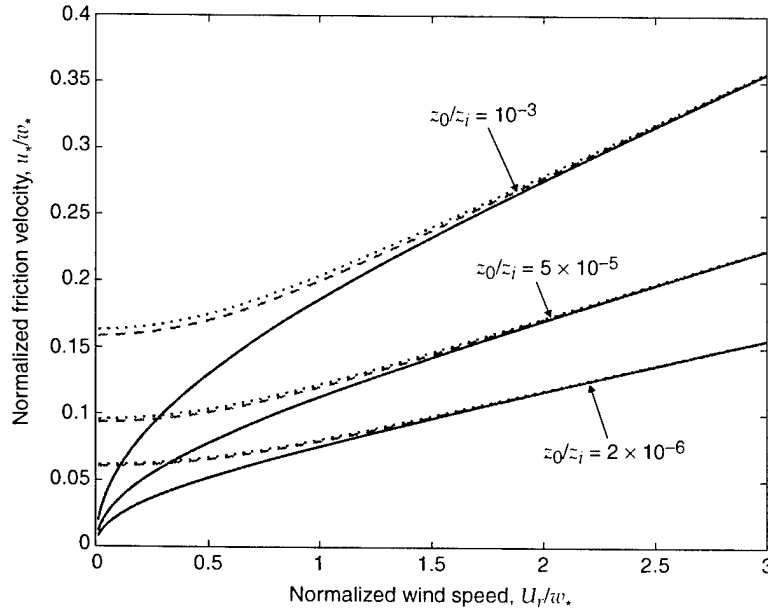
The global friction velocity is compared to the averaged local value, $\langle u_{*L} \rangle$, in figure 3. For wind speeds U_r larger than w_* , the global and averaged local values are nearly the same. As the wind speed approaches zero, however, the global value vanishes, whereas the local average becomes constant. This asymptote is the minimum friction velocity recognized by Businger (1973a,b), Schumann (1988), and others. Also shown on the figure are approximate results for $\langle u_{*L} \rangle$ based on the average local wind speed at the reference height, $\langle U_L \rangle$, as given by equation (12). I found these results by solving equation (25) for u_{*L} , except that I replaced the local wind speed by $\langle U_L \rangle$. The resulting value of u_{*L} will be designated as $u_{*,\text{eff}}$ in the remainder of this report; that is,

$$\langle U_L \rangle = \frac{u_{*,\text{eff}}}{\kappa} h_M \left(\frac{z_r}{L_{\text{eff}}}, \frac{z_0}{L_{\text{eff}}} \right). \quad (47)$$

where $L_{\text{eff}} = -u_{*,\text{eff}} T_s / (\kappa g Q_s)$. The figure demonstrates that $u_{*,\text{eff}}$ is a very good approximation to the actual value of $\langle u_{*L} \rangle$ for all reasonable combinations of U_r/w_* and z_0/z_i . This observation lends support to the analyses of Godfrey and Beljaars (1991) and Grachev et al (1998) who use an effective value for u_* based on the mean wind speed.

Let us analyze now in more detail the vanishing mean wind speed, using approximate forms for $\phi_M(\zeta)$ that will allow us to obtain an analytical solution. Simple approximations for $\phi_M(\zeta)$ are available for the two limiting cases of neutral and free-convection stability. It may seem obvious, at first glance, that we should use the free-convection stability limit, namely $\phi_M(\zeta) \simeq (-a_M \zeta)^{-1/3}$ (Carl et al, 1973; Kader and Yaglom, 1990). However, we should keep in mind that even when the mean wind vanishes, there

Figure 3. Global (solid lines) and average local (dashed lines) friction velocity as a function of vector-average wind speed at reference height, U_r . Dotted lines are an approximation for average local friction velocity based on mean local wind speed, $\langle U_L \rangle$.



is still local shear from the gusts. Sykes et al (1993) actually based their analysis on locally neutral profiles. So, to be careful, we should calculate the neutral and free-convection stability limits for the local wind profiles separately and then compare the results to numerical calculations made with the full Monin-Obukhov similarity equation for $\phi_M(\zeta)$.

For the neutral limit, $\phi_M(\zeta) = 1$, and one has (app B, eq (B-26))

$$\frac{\langle u_{*L} \rangle}{w_*} = \frac{\sqrt{\pi} \beta \kappa}{2 \ln(z_r/z_0)}. \quad (48)$$

Replacing the constants with their numerical values results in

$$\frac{\langle u_{*L} \rangle}{w_*} = 0.34 \ln^{-1} \left(\frac{z_i}{10z_0} \right). \quad (49)$$

For the free convection limit (app B, eq (B-34)),

$$\frac{\langle u_{*L} \rangle}{w_*} = \frac{\Gamma(5/4) \beta^{1/2} \kappa^{2/3} a_M^{1/6}}{\sqrt{3}} \left[\left(\frac{z_i}{z_0} \right)^{1/3} - \left(\frac{z_i}{z_r} \right)^{1/3} \right]^{-1/2}. \quad (50)$$

Replacing the constants with their numerical values,

$$\frac{\langle u_{*L} \rangle}{w_*} = 0.42 \left[\left(\frac{z_i}{z_0} \right)^{1/3} - 2.2 \right]^{-1/2}. \quad (51)$$

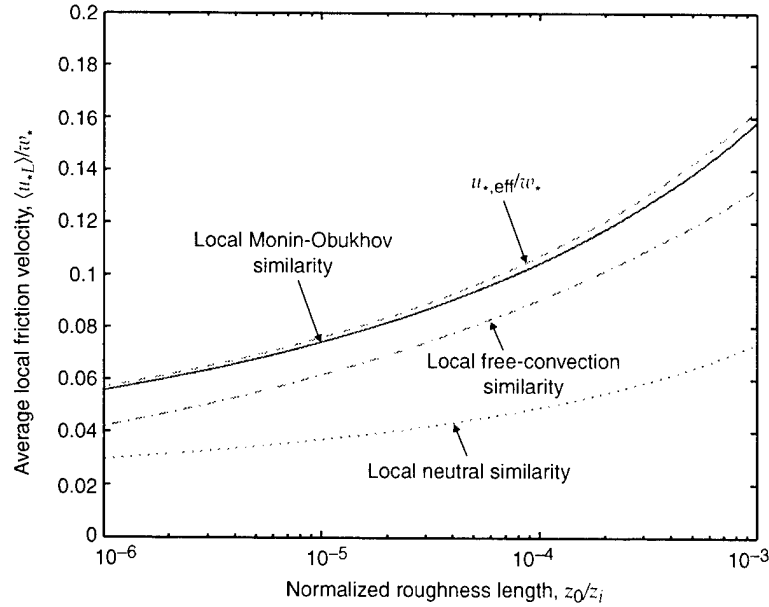
Generally, z_i is much larger than z_0 , and we may neglect the second term in the square brackets, leaving

$$\frac{\langle u_{*L} \rangle}{w_*} = 0.42 \left(\frac{z_i}{z_0} \right)^{-1/6}. \quad (52)$$

This result is very similar to an approximation derived by Schumann (1988) (his eq (37)), the only difference being the numerical coefficient, which Schumann determined as 0.52. It is reassuring that the approach in this report, based on a statistical model for the gusts, yields nearly the same results as Schumann's model, which is based on an entirely different approach involving bulk approximations.

Figure 4 compares a numerical evaluation of the average friction velocity, based on local application of the full Monin-Obukhov equation (15) for $\phi_M(\zeta)$, to the two approximate analytical solutions, equations (49) and (51). Also shown is $u_{*,\text{eff}}$ from equation (47), which is observed to be an excellent proxy for $\langle u_{*L} \rangle$ throughout the range of roughnesses. The approximation that the profiles under the gusts locally obey free-convection similarity produces better agreement with the full local Monin-Obukhov evaluation than does neutral similarity. For unrealistically small roughness lengths (not shown on the figure), the neutral similarity curve does eventually become the better approximation. We conclude that in conditions of vanishing wind speed, the local profiles more closely resemble their free-convection forms than their neutral ones.

Figure 4. Local average friction velocity as a function of roughness length for vanishing mean wind. Three curves are based on different methods for calculating local wind profiles under large eddies.



3.2 Mean Profiles

Because Monin-Obukhov similarity is widely used to model the mean vertical profiles of wind and temperature, an important practical matter is whether the local-equilibrium model implies any significant, systematic violations of global Monin-Obukhov similarity. More precisely, when the mean gradients are normalized by u_* and T_* as in equations (13) and (14), are they still universal functions of z/L ? We might furthermore ask, even if the global application of Monin-Obukhov similarity is tenuous, can empirically *fitted* values for u_* and T_* be devised that still produce good agreement with atmospheric data?

Starting with the first question, let us write down equations for the mean wind and temperature gradients in the context of local equilibrium. Applying equations (13) and (14) locally and then taking the global average, yields

$$\frac{d\langle U \rangle}{dz} = \frac{1}{\kappa z} \left\langle u_{*L} \cos \theta \phi_M \left(\frac{z}{L_L} \right) \right\rangle, \quad \text{and} \quad (53)$$

$$\frac{d\langle T \rangle}{dz} = -\frac{P_t Q_s}{\kappa z} \left\langle u_{*L}^{-1} \phi_H \left(\frac{z}{L_L} \right) \right\rangle. \quad (54)$$

Next, when we nondimensionalize by multiplying with $\kappa z/u_*$ and $-\kappa z u_*/P_t Q_s$, we have

$$\frac{\kappa z}{u_*} \frac{d\langle U \rangle}{dz} = \left\langle u_{*L} \cos \theta \phi_M \left(\frac{z}{L_L} \right) \right\rangle \langle u_{*L}^2 \cos \theta \rangle^{-1/2}, \quad \text{and} \quad (55)$$

$$-\frac{\kappa z u_*}{P_t Q_s} \frac{d\langle T \rangle}{dz} = \left\langle u_{*L}^{-1} \phi_H \left(\frac{z}{L_L} \right) \right\rangle \langle u_{*L}^2 \cos \theta \rangle^{1/2}. \quad (56)$$

Plots of the nondimensional wind and temperature gradients calculated from these equations are shown in figures 5 and 6. Four different values

Figure 5.
Nondimensional
wind gradient
 $(z\kappa/u_*) (d\langle U \rangle / dz)$ as a
function of $\zeta = -z/L$.

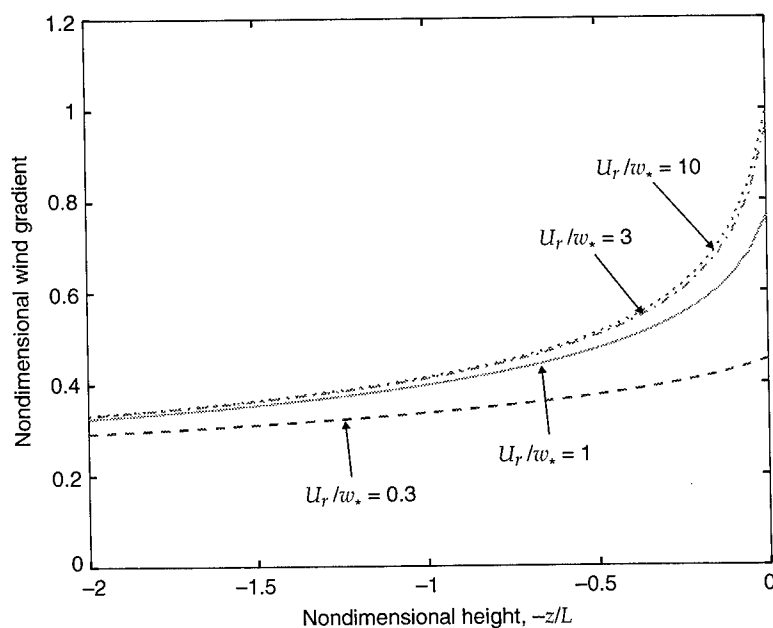
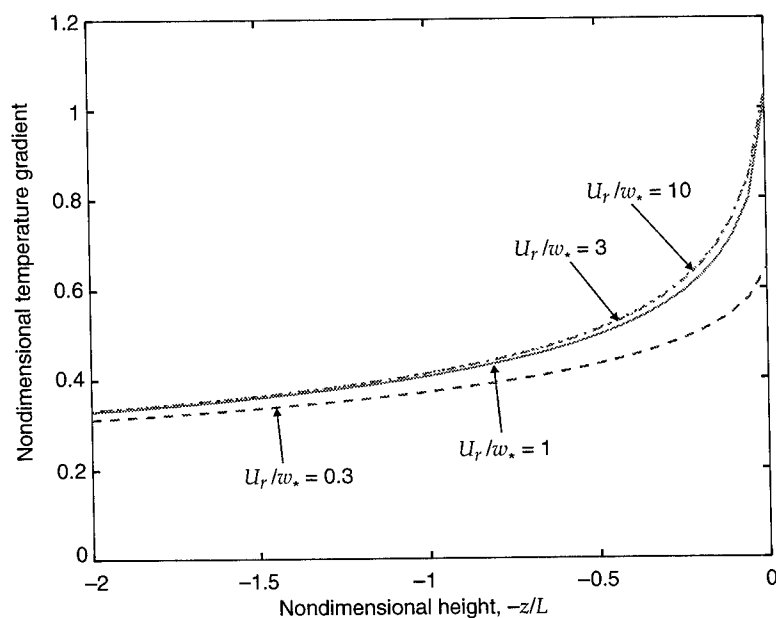


Figure 6.
Nondimensional
temperature gradient
 $(-z\kappa u_*/P_t Q_s) (d\langle T \rangle / dz)$ as a function
of $\zeta = -z/L$.



of the ratio U_r/w_* are shown: 0.3, 1, 3, and 10. For a surface roughness $z_0/z_i = 10^{-4}$, these four values correspond to $-z_i/L = \kappa (w_*/u_*)^3 = 1200, 190, 26,$ and 1.6 . The first value is extremely convective and probably rare for the atmosphere. The second represents a fair summer day over land.

For the global application of Monin-Obukhov similarity to be valid, the curves in figures 5 and 6 can depend only on z/L ; that is, for all values of U_r/w_* , they must collapse onto a single curve. Clearly this does not happen. Substantial deviations from global Monin-Obukhov similarity are found when $U_r/w_* \leq 1$ for the wind gradient and $U_r/w_* \leq 0.3$ for the temperature gradient. The dependence of the nondimensional gradients on U_r/w_*

may explain some of the scatter in measurements such as those made by Businger et al (1971) and by Högström (1988). The data should be reexamined for dependence on the inversion height.

Besides U_r/w_* , the local-equilibrium theory also predicts a dependence of the nondimensional gradients on z_0/z_i . By performing numerical evaluations, I found this effect to be quite insignificant, being most discernable when $U_r/w_* \ll 1$.

Next we turn to the question of whether we can still fit equations (16) and (17) to surface-layer data with good results, even when there is a breakdown in the global application of Monin-Obukhov similarity. This amounts to selecting values for u_* and T_* , possibly different from their actual values, to fit the profiles at some set of sensor heights. Then we assess whether these fitted values produce good agreement with the actual overall profiles.

To gain some insight into how the fitted values for u_* and T_* can differ from their actual values, consider the equations for the ensemble mean profiles derived from the local-equilibrium theory. The wind profile follows directly from equation (22):

$$\langle U(z) \rangle = \frac{1}{\kappa} \left\langle u_{*L} \cos \theta h_M \left(\frac{z}{L_L}, \frac{z_0}{L_L} \right) \right\rangle. \quad (57)$$

The mean temperature profile follows by averaging equation (21), with $\langle T(z) \rangle = \langle \langle T(z) \rangle_L \rangle$:

$$\langle T(z) \rangle = T(z_h) + \frac{P_t}{\kappa} \left\langle T_{*L} h_H \left(\frac{z}{L_L}, \frac{z_h}{L_L} \right) \right\rangle. \quad (58)$$

Because h_M and h_H are complicated functions of u_{*L} , it is not possible to analytically derive a general equation for effective values of u_* and T_* . For the idealized situation where neutrally stable conditions prevail locally, h_M and h_H are logarithmic, and the two preceding equations become

$$\langle U(z) \rangle = \frac{1}{\kappa} \ln \frac{z}{z_0} \langle u_{*L} \cos \theta \rangle, \quad \text{and} \quad (59)$$

$$\langle T(z) \rangle = T(z_h) - \frac{P_t Q_s}{\kappa} \ln \frac{z}{z_h} \langle u_{*L}^{-1} \rangle. \quad (60)$$

Since the mean profile in neutral conditions, according to the global-equilibrium theory, is $\langle U(z) \rangle = (u_*/\kappa) \ln(z/z_0)$, the first of these equations implies simply that $\langle u_{*L} \cos \theta \rangle$ plays the role of an effective value for u_* . If the gusts are relatively strong and randomly oriented, $\langle u_{*L} \cos \theta \rangle$ can be much smaller than $\langle u_{*L} \rangle$. Similarly, $-Q_s \langle u_{*L}^{-1} \rangle$ plays the role of an effective temperature scale in place of $T_* = -Q_s/u_*$ in the global theory.

Turning now to the other limiting approximation, where free convection prevails locally, one can show (app B) that $\langle U(z) \rangle \propto \langle u_{*L}^2 \cos \theta \rangle$. Since the global-equilibrium model predicts $\langle U(z) \rangle \propto u_*^2$, and $u_*^2 = \langle u_{*L}^2 \cos \theta \rangle$ (eq (46)), the effective friction velocity in free convection is the same as the

actual friction velocity. In regards to the temperature profile, it becomes independent of u_* in free convection (see, for example (Kader and Yaglom, 1990)). Therefore in this extreme, there is no local variability in the temperature profiles, and $T_* = -Q_s/u_*$ can be used as an effective temperature scale.

To elucidate these ideas, let us consider an example atmospheric boundary layer with $w_* = 3$ m/s, $z_0 = 10^{-5}$ m, and $z_i = 1000$ m ($Q_s = 0.81$ Ks/m). The wind speed U_r is varied. For each value of U_r , fitted values of u_* and T_* are determined by matching equations (13) and (14) to the wind speed and temperature at 10-m height. Figure 7 shows the resulting ratio of the fitted value of u_* ($u_{*,\text{fit}}$) to the actual value. For large U_r/w_* , the fitted friction velocity is the same as the actual value. As U_r/w_* becomes less than about 10, $u_{*,\text{fit}}$ becomes less than the actual value, as would be anticipated from the preceding discussion. Surprisingly, as $U_r/w_* \rightarrow 0$, the ratio approaches a constant value smaller than one. Based on the preceding discussion, the asymptote should equal one. The reason behind this apparent discrepancy is that the free-convection limit is never truly attained. The gusts prevent the turbulence from being in such a state locally.

Figures 8 and 9 illustrate agreement between wind and temperature profiles from the local-equilibrium model to those based on fitted values for u_* and T_* . Plotted are the ratios $[U_{\text{fit}}(z) - \langle U(z) \rangle] / \langle U(z) \rangle$ and $[T_{\text{fit}}(z) - \langle T(z) \rangle] / \langle T(z) \rangle$ for $z = 2$ m and $z = 100$ m, where $U_{\text{fit}}(z)$ and $T_{\text{fit}}(z)$ are the profiles calculated by fitting u_* and T_* to measurements at $z = 10$ m. Also shown are $[U_{\text{glob}}(z) - \langle U(z) \rangle] / \langle U(z) \rangle$ and $[T_{\text{glob}}(z) - \langle T(z) \rangle] / \langle T(z) \rangle$ for $z = 2$ m and $z = 100$ m, where $U_{\text{glob}}(z)$ and $T_{\text{glob}}(z)$ are the profiles calculated from the global-equilibrium model. The profiles calculated from the fitted values are always in good agreement (relative error less than about 4%) with the local-equilibrium model, even

Figure 7. Ratio of friction velocity determined by fitting measurements at 10-m height to actual value determined from local-equilibrium model.

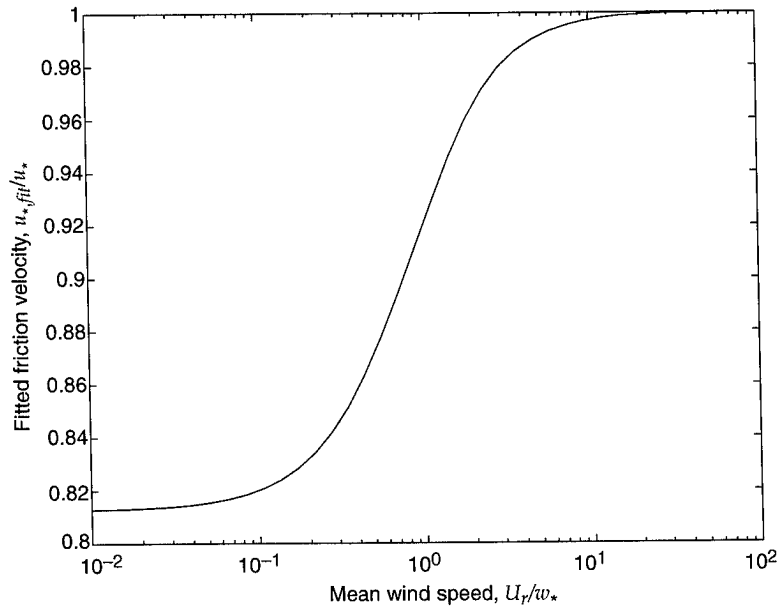


Figure 8. Relative error (in %) between wind speed profile in local-equilibrium model and a profile determined by fitting u_* and T_* to measurements at 10-m height. Errors are shown for 2- and 100-m heights. Also shown are relative errors for global Monin-Obukhov similarity based on actual values of u_* and T_* .

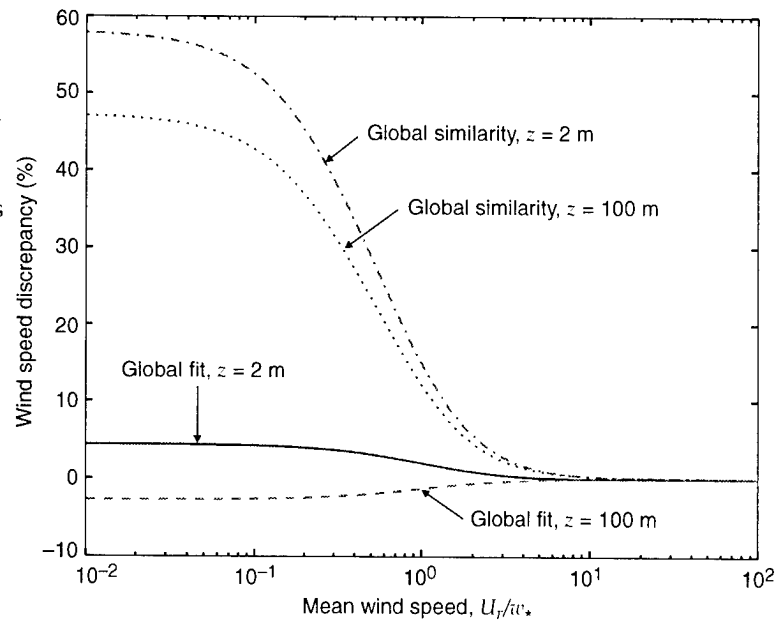
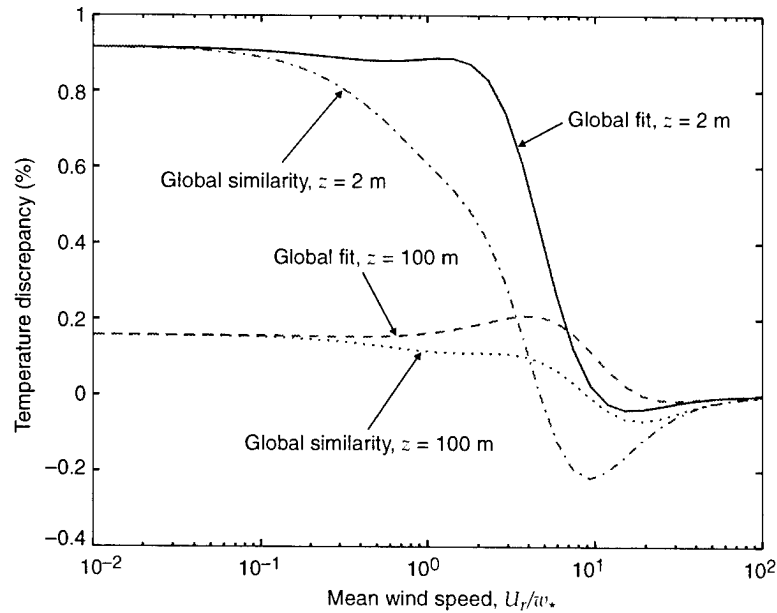


Figure 9. Same as figure 8, except for temperature profile.



for very small U_r/w_* . The global-equilibrium profiles for the wind speed are in poor agreement with the local-equilibrium model, although agreement for the temperature profiles is quite good. The reason for this behavior was mentioned earlier: the local temperature profiles are independent of u_* in highly convective conditions, and therefore the global and local models match in this case. In interpreting the results for the wind profiles, one should keep in mind that values for $U_r/w_* < 1$ are unusual for the atmosphere. Even for $U_r/w_* = 1$, though, the global-equilibrium model can

be off by more than 10 percent. Application of global similarity theory to the wind profiles in highly convective atmospheric conditions is therefore very tenuous, although when fitted values for u_* and T_* are used in place of the actual ones, the theory can be made to work fairly well.

3.3 Temperature Variance

In this section, I explore the implications of the local-equilibrium model for the temperature variance. The temperature variance is defined as

$$\sigma_T^2(z) = \langle [T(z) - \langle T(z) \rangle]^2 \rangle. \quad (61)$$

Previous studies, based on a global similarity approach, have found the surface-layer temperature variance in neutral conditions to be about $4.0T_*^2$ (e.g., Stull's (1988) equation 9.5.3k). In freely convective conditions, the previous studies suggest $\sigma_T^2 = 0.90T_*^2(-z/L)^{-2/3}$ (Kaimal et al, 1976; Caughey and Palmer, 1979). The following equation smoothly interpolates between these two limits:

$$\frac{\sigma_T^2}{T_*^2} = 4.0 \left[1 + 4.4 \left(-\frac{z}{L} \right)^{2/3} \right]^{-1}. \quad (62)$$

Note that the temperature fluctuations are entirely "small scale"; that is, since neither w_* nor z_i appear in the previous equation, the large-scale convective eddies have not previously been observed to affect the temperature variance.

In the context of local equilibrium, the large convective gusts can modify the temperature variance in two ways. First, they can *directly* vary the temperature through local adjustments to the vertical profile. Second, they can *indirectly* affect the temperature variance by locally modulating σ_T^2 through changes in u_{*L} . Let us decompose the temperature as follows:

$$T = \langle T \rangle + T_G + t, \quad (63)$$

where T_G is the change induced directly by the gusts and t represents the small-scale fluctuations obeying equation (62), except with local scales replacing the global ones. The variance is therefore

$$\sigma_T^2 = \langle (T_G + t)^2 \rangle = \langle T_G^2 \rangle + 2 \langle T_G t \rangle + \langle t^2 \rangle. \quad (64)$$

Let us decompose t as

$$t = \sigma_{T,L} \xi, \quad (65)$$

where ξ is a random variable having zero mean and unit variance. The factor $\sigma_{T,L}$ scales the variance locally in response to the gusts. Having factored out $\sigma_{T,L}$, I can now consider the random variable ξ a process independent from the gusts. As a result, the direct and indirect contributions separate from each other:

$$\sigma_T^2 \simeq \langle T_G^2 \rangle + 2 \langle T_G \sigma_{T,L} \rangle \langle \xi \rangle + \langle \sigma_{T,L}^2 \rangle \langle \xi^2 \rangle = \langle T_G^2 \rangle + \langle \sigma_{T,L}^2 \rangle. \quad (66)$$

Let us first consider the direct contribution, $\langle T_G^2 \rangle$. By definition, $T_G = \langle T(z) \rangle_L - \langle T(z) \rangle$. From equation (21) (with z_r appearing in place of z_h , as discussed at the end of sect. 2.2),

$$T_G = \frac{P_t}{\kappa} \left[T_{*L} h_H \left(\frac{z}{L_L}, \frac{z_r}{L_L} \right) - \left\langle T_{*L} h_H \left(\frac{z}{L_L}, \frac{z_r}{L_L} \right) \right\rangle \right], \quad (67)$$

and therefore

$$\langle T_G^2 \rangle = \left(\frac{P_t}{\kappa} \right)^2 \left[\left\langle T_{*L}^2 h_H^2 \left(\frac{z}{L_L}, \frac{z_r}{L_L} \right) \right\rangle - \left\langle T_{*L} h_H \left(\frac{z}{L_L}, \frac{z_r}{L_L} \right) \right\rangle^2 \right]. \quad (68)$$

Substituting $T_{*L} = -Q_s/u_{*L}$, and normalizing with $\theta_* = Q_s/w_*$, we have

$$\frac{\langle T_G^2 \rangle}{\theta_*^2} = \left(\frac{P_t}{\kappa} \right)^2 \left[\left\langle \left(\frac{w_*}{u_{*L}} \right)^2 h_H^2 \left(\frac{z}{L_L}, \frac{z_r}{L_L} \right) \right\rangle - \left\langle \left(\frac{w_*}{u_{*L}} \right) h_H \left(\frac{z}{L_L}, \frac{z_r}{L_L} \right) \right\rangle^2 \right]. \quad (69)$$

Since z_r/L_L is proportional to $(w_*/u_{*L})^3$, the right-hand side is a function of u_{*L}/w_* and z/L , and we know from the theorem (35) that $\langle T_G^2 \rangle / \theta_*^2$ must depend on the dimensionless ratios U_r/w_* , z/z_i , and z_0/z_i .

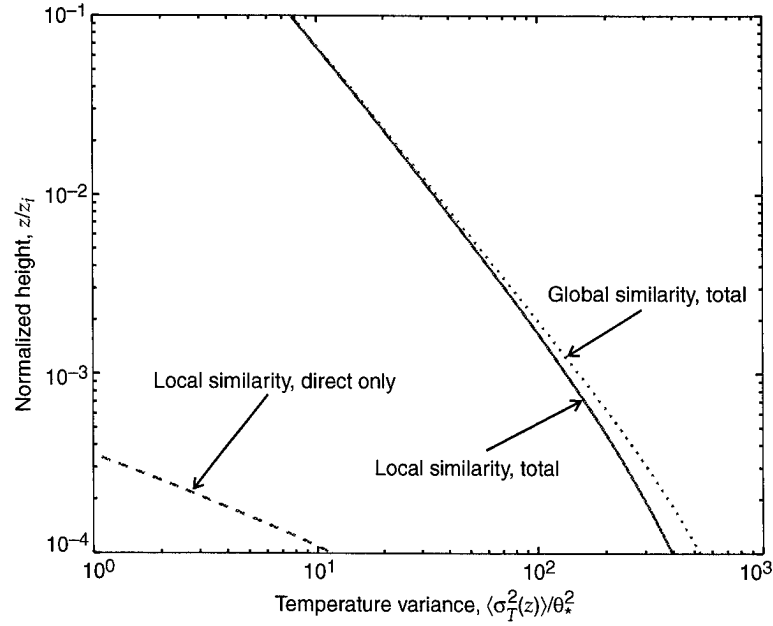
With respect to the indirect contribution, the local temperature variance is the same as equation (62), except that T_{*L} replaces T_* and L_L replaces L . Making these replacements and normalizing the local friction velocity by w_* , we have

$$\frac{\sigma_{T,L}^2}{\theta_*^2} = 4.0 \left(\frac{w_*}{u_{*L}} \right)^2 \left[1 + 4.4 \left(-\frac{z}{L_L} \right)^{2/3} \right]^{-1}. \quad (70)$$

Similarly to the direct contribution, we know from equation (35) that $\langle \sigma_{T,L}^2 \rangle / \theta_*^2$ must depend on the dimensionless ratios U_r/w_* , z/z_i , and z_0/z_i .

The local-equilibrium model prediction for $U_r/w_* = 0.3$ is broken down and compared to global similarity in figure 10. The direct effect of the gusts (local modification of the vertical temperature profile) is insignificant. The variance is almost entirely locally generated. But more importantly, the local and global similarity models are nearly identical, even though this case is highly convective by atmospheric standards. This behavior can be explained by the fact that the convective contribution to the variance, $0.90 T_{*L}^2 (-z/L_L)^{-2/3} = 0.90 (T_0 Q_s^2 / \kappa g z)^{2/3}$, is independent of u_{*L} . Therefore the gusts have a vanishing local effect in highly convective conditions. I examined several other combinations of U_r/w_* and z_0/z_i and concluded that the gusts cause no significant modifications to the temperature variance for ordinary atmospheric conditions. The local-equilibrium model is therefore consistent with atmospheric observations, which have so far shown no discernable dependence of the temperature variance on the large-scale convective eddies.

Figure 10. Temperature variance predictions for $U_r/w_* = 0.3$. Solid curve is total prediction from local-equilibrium model. Dashed curve is contribution to local-equilibrium model caused directly by gusts. Dotted curve is total prediction from global-equilibrium model.



3.4 Vertical Velocity Variance

Previous experimental studies have shown that the vertical velocity variance, like the temperature variance, is concentrated at small scales. Panofsky et al (1977) found the vertical velocity variance in the surface layer to be well represented by

$$\frac{\sigma_w^2}{u_*^2} = 1.6 + 2.9 \left(-\frac{z}{L} \right)^{2/3}, \quad (71)$$

or, equivalently, by

$$\frac{\sigma_w^2}{w_*^2} = 1.6 \left(\frac{u_*}{w_*} \right)^2 + 1.6 \left(\frac{z}{z_i} \right)^{2/3}. \quad (72)$$

Unlike the mean temperature profile, the mean vertical velocity profile exhibits no height dependence: it is essentially zero at all heights in the surface layer. Therefore, in developing a local-equilibrium model, I should set the large-scale (direct) contribution to the vertical velocity to zero. We have simply $\sigma_w^2 = \langle \sigma_{w,L}^2 \rangle$, where $\sigma_{w,L}^2$ is given by equation (72), with u_{*L} replacing u_* :

$$\frac{\sigma_w^2}{w_*^2} = 1.6 \frac{\langle u_{*L}^2 \rangle}{w_*^2} + 1.6 \left(\frac{z}{z_i} \right)^{2/3}. \quad (73)$$

Figures 11 and 12 show the vertical velocity variance calculated from the global- and local-equilibrium models. The figures are for roughness lengths of $z_0 = 10^{-5}z_i$ and $z_0 = 10^{-3}z_i$, respectively. The ratio of the local prediction (eq (73)) to the global prediction (eq (72)) is plotted. The local and global predictions start to differ substantially when $U_r/w_* \leq 1$, particularly for the rough surface. In fact, the variance nearly doubles near the ground

Figure 11. Ratio of vertical velocity variance (σ_w^2) predicted by local-equilibrium model to global similarity prediction, for a smooth surface ($z_0/z_i = 10^{-5}$).

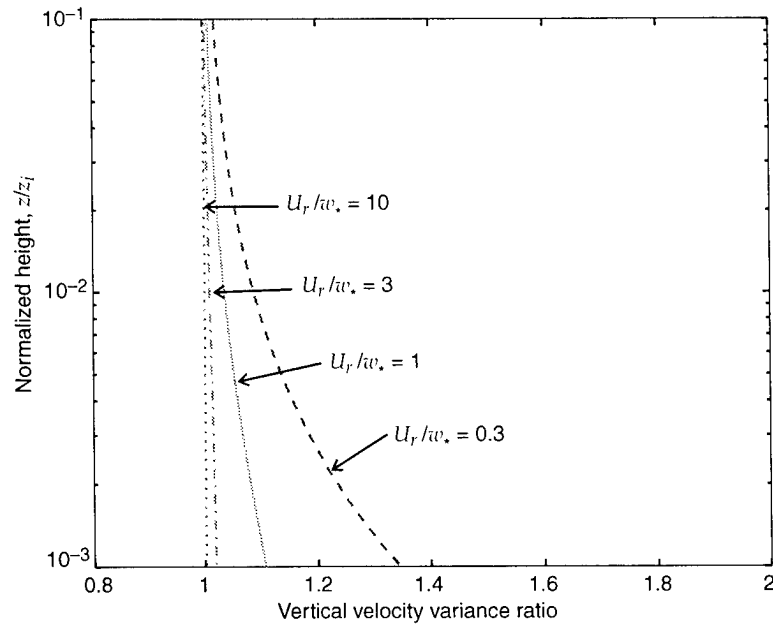
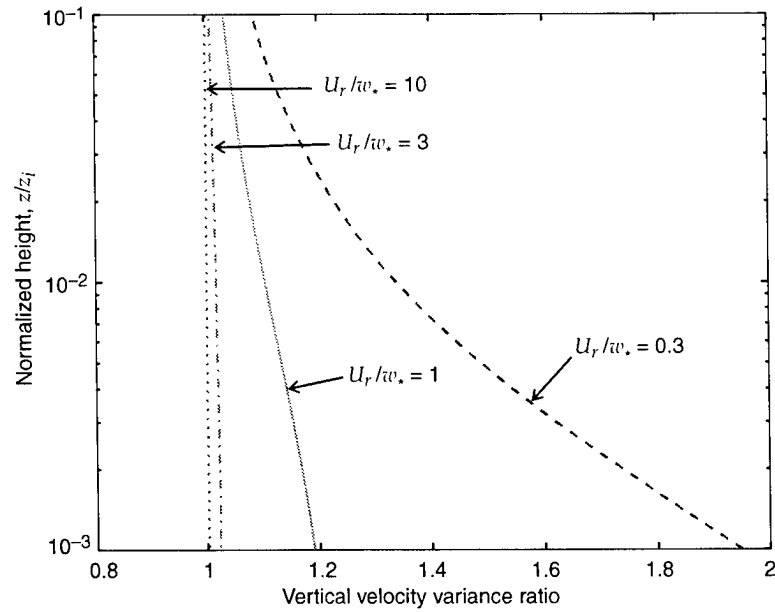


Figure 12. Same as figure 11, but for a rough surface ($z_0/z_i = 10^{-3}$).



for the rough surface when $U_r/w_* = 0.3$. The cause is mechanical turbulence generated locally by gusts.

Let us analyze the behavior of the vertical velocity variance for small U_r/w_* in more detail. Recall from section 3.1 that, in analyzing statistics of u_{*L} , the free-convection approximation for the profiles was found to be more satisfactory than the neutral approximation. Applying the free-convection approximation to the local wind profiles, we have from equation (B-34)

$$\frac{\langle u_{*L}^2 \rangle}{w_*^2} = \frac{\sqrt{\pi}\beta\kappa^{4/3}a_M^{1/3}}{6} \left[\left(\frac{z_i}{z_0} \right)^{1/3} - \left(\frac{z_i}{z_r} \right)^{1/3} \right]^{-1}. \quad (74)$$

When I substitute numerical values for the constants and make the additional approximation $z_0 \ll z_r$, the previous equation becomes

$$\frac{\langle u_{*L}^2 \rangle}{w_*^2} = 0.19 \left(\frac{z_0}{z_i} \right)^{1/3}. \quad (75)$$

Hence, from equation (73),

$$\frac{\sigma_w^2}{w_*^2} = 0.31 \frac{\langle u_{*L}^2 \rangle}{w_*^2} + 1.6 \left(\frac{z}{z_i} \right)^{2/3}. \quad (76)$$

The following approximate expression interpolates smoothly between the mechanical and free-convection limits:

$$\sigma_w^2 = 1.6u_*^2 + \left[0.31 \left(\frac{z_0}{z_i} \right)^{1/3} + 1.6 \left(\frac{z}{z_i} \right)^{2/3} \right] w_*^2. \quad (77)$$

The only difference between this equation and the one from Panofsky et al (1977) (eq 72) is the extra term, $0.31 w_*^2 (z_0/z_i)^{1/3}$. This formula is plotted and compared to the local equilibrium prediction in figure 13. We see that the approximate formula works best for $U_r/w_* \ll 1$ but is still satisfactory for moderate U_r/w_* .

3.5 Horizontal Velocity Variance

Analogously to the temperature, the velocity component in the along-wind (x -) direction can be decomposed as follows:

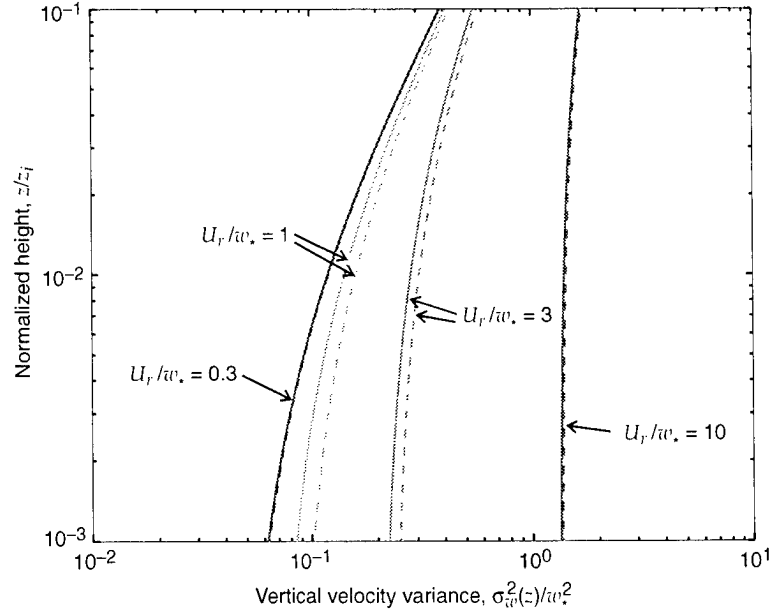
$$U = \langle U \rangle + G_x + u, \quad (78)$$

where u contains the small-scale fluctuations filtered out by the local averaging operation. Therefore we have for the variance

$$\sigma_u^2 \equiv \langle (U - \langle U \rangle)^2 \rangle = \langle G_x^2 \rangle + 2 \langle G_x u \rangle + \langle u^2 \rangle. \quad (79)$$

In principle, we could devise a formula for the horizontal velocity variance similar to equation (62) for the temperature variance, interpolating between the neutral and free-convection limits. However, the free-convection limit

Figure 13. Comparison of approximate formula, equation (77) (dashed lines), to local-equilibrium model prediction (solid lines). Calculations are for a rough surface ($z_0/z_i = 10^{-3}$).



for the horizontal velocity variance has not yet been conclusively observed in the atmosphere. Apparently, the contributions to the variance from mechanical turbulence and the large-scale convective eddies nearly always dominate any contributions from the smaller (z -) scale convective eddies. (See, for example, the discussion in Kader and Yaglom (1990, pp 651–652).) Therefore only the contribution from purely mechanical turbulence (the neutral limit) need be included in the formulation for u . Locally, these fluctuations scale in proportion to u_{*L} .

Variances for shear turbulence also depend on the direction relative to the mean wind. Representative values for the along-wind and crosswind standard deviations are $2.4 u_*$ and $1.9 u_*$, respectively (Panofsky and Dutton, 1984). In the context of local equilibrium, we therefore model u as

$$u = (2.4 \cos \theta + 1.9 \sin \theta) u_{*L} \xi, \quad (80)$$

where ξ is a zero-mean, unit-variance random variable as in the previous section. Based on the assumption that ξ is independent of the gusts, the cross term in equation (79) vanishes, leaving

$$\sigma_u^2(z) = \langle G_x^2(z) \rangle + 5.8 \langle u_{*L}^2 \cos^2 \theta \rangle + 3.6 \langle u_{*L}^2 \sin^2 \theta \rangle. \quad (81)$$

A similar treatment for the crosswind variance results in

$$\sigma_v^2(z) = \langle G_y^2(z) \rangle + 5.8 \langle u_{*L}^2 \sin^2 \theta \rangle + 3.6 \langle u_{*L}^2 \cos^2 \theta \rangle. \quad (82)$$

From equations (35) and (40), we know that $\langle G_x^2(z) \rangle$ and $\langle G_y^2(z) \rangle$ in equations (81) and (82), after nondimensionalization with w_*^2 , depend on the ratios U_r/w_* , z/z_i , and z_0/z_i . The quantities $\langle u_{*L}^2 \cos^2 \theta \rangle / w_*^2$ and $\langle u_{*L}^2 \sin^2 \theta \rangle / w_*^2$ are independent of height and are therefore functions of U_r/w_* and z_0/z_i . We conclude that $\sigma_u^2(z)/w_*^2$ and $\sigma_v^2(z)/w_*^2$ depend overall on U_r/w_* , z/z_i , and z_0/z_i .

If we were to neglect the height dependence of $\langle G_x^2(z) \rangle$ and $\langle G_y^2(z) \rangle$ and set $\langle u_{*L}^2 \rangle = u_*^2$ and $\theta = 0$, the previous expressions would reduce to $\sigma_u^2 = 0.45w_*^2 + 5.8u_*^2$ and $\sigma_v^2 = 0.45w_*^2 + 3.6u_*^2$. This simple addition of variances from large-scale convective gusts and mechanical turbulence has been previously suggested by Panofsky et al (1977), Højstrup (1982), Wilson and Thomson (1994), and Peltier et al (1996). But equations (81) and (82) incorporate additional phenomena not present in the previous formulations. Most significantly, they include height dependence of the gust structure, and the conversion of energy from the gusts to local mechanical turbulence.

To better understand the behavior of equations (81) and (82), let us determine explicit results for the idealized cases of local neutral and free-convection profiles underneath the gusts. For the neutral limit, equation (20) yields the two component equations

$$\frac{u_{*L}}{\kappa} \ln \frac{z}{z_0} \cos \theta = \langle U(z) \rangle + G_x(z) \quad \text{and} \quad (83)$$

$$\frac{u_{*L}}{\kappa} \ln \frac{z}{z_0} \sin \theta = G_y(z) . \quad (84)$$

Squaring both equations and taking expected values, we have

$$\langle G_x^2(z) \rangle = \frac{1}{\kappa^2} \ln^2 \frac{z}{z_0} \langle u_{*L}^2 \cos^2 \theta \rangle - \langle U(z) \rangle^2 \quad \text{and} \quad (85)$$

$$\langle G_y^2(z) \rangle = \frac{1}{\kappa^2} \ln^2 \frac{z}{z_0} \langle u_{*L}^2 \sin^2 \theta \rangle , \quad (86)$$

where

$$\langle U(z) \rangle = \frac{1}{\kappa} \ln \frac{z}{z_0} \langle u_{*L} \cos \theta \rangle . \quad (87)$$

The various moments involving u_{*L} and θ are evaluated in appendix B as equations (B-20), (B-22), and (B-23). Incorporating those results, we have

$$\sigma_u^2(z) = \frac{5.8\kappa^2 U_r^2}{\ln^2(z_r/z_0)} + \frac{\beta^2 w_*^2}{2 \ln^2(z_r/z_0)} [\ln^2(z/z_0) + 9.4\kappa^2] . \quad (88)$$

A similar treatment for the crosswind variance results in the same formula but with 3.6 replacing 5.8 in the first term. In equation (88), the first term on the right arises from shear production by the mean wind. The first and second terms in the square brackets represent the direct effect of the gusts and local shear production, respectively. Note that the local shear production is height independent.

Now let us reanalyze the problem in the free-convection limit. If the mean wind speed is negligible, $\langle u_{*L}^2 \cos^2 \theta \rangle$ and $\langle u_{*L}^2 \sin^2 \theta \rangle$ must both equal $\langle u_{*L}^2 \rangle / 2$, leaving

$$\sigma_{u,v}^2(z) = 0.5 \langle G^2(z) \rangle + 4.7 \langle u_{*L}^2 \rangle . \quad (89)$$

Away from the influence of the ground, one would have $\sigma_{u,v}^2 \approx 0.5 \langle G^2(z_r) \rangle = 0.45w_*^2$. Very near the ground, however, surface drag diminishes the gust velocity, so that $\langle G^2(z) \rangle$ must become small. Shear forces can

counteract this decrease in the variance by locally enhancing $\langle u_{*L}^2 \rangle$. In the limit of large $-z/L_L$ and $-z_0/L_L$, one has from equations (13) and (15)

$$U_L(z) = G(z) \simeq \frac{3u_{*L}^2}{\kappa^{4/3}a_M^{1/3}w_*} \left[\left(\frac{z_i}{z_0} \right)^{1/3} - \left(\frac{z_i}{z} \right)^{1/3} \right] \quad (90)$$

so that

$$\langle G^2(z) \rangle = \left(\frac{3}{\kappa^{4/3}a_M^{1/3}w_*} \right)^2 \left[\left(\frac{z_i}{z_0} \right)^{1/3} - \left(\frac{z_i}{z} \right)^{1/3} \right]^2 \langle u_{*L}^4 \rangle. \quad (91)$$

Therefore, to evaluate equation (89), we need $\langle u_{*L}^2 \rangle$ and $\langle u_{*L}^4 \rangle$. These can be found in appendix B as equation (B-34). One subsequently finds that

$$\frac{\sigma_{u,v}^2(z)}{w_*^2} = \frac{\beta^2}{2} \left[\frac{1 - (z_0/z)^{1/3}}{1 - (z_0/z_r)^{1/3}} \right]^2 + \frac{4.7\sqrt{\pi}\beta\kappa^{4/3}a_M^{1/3}}{6} \left(\frac{z_0}{z_i} \right)^{1/3}. \quad (92)$$

Substituting numerical values for the constants, we have

$$\frac{\sigma_{u,v}^2(z)}{w_*^2} = 0.45 \left[\frac{1 - (z_0/z)^{1/3}}{1 - (z_0/z_r)^{1/3}} \right]^2 + 0.89 \left(\frac{z_0}{z_i} \right)^{1/3}. \quad (93)$$

The first term on the right is the direct effect of the large-scale gusts, whereas the second term represents local shear production. These terms are analogous to the second and third in equation (88). Equation (93) differs from the usual one for the horizontal velocity variance in a convective boundary layer, namely $\sigma_{u,v}^2(z) = 0.45w_*^2$. These differences are significant near the ground, particularly over rough surfaces. If $z_0 = 10^{-3}z_i$, the local shear production term equals $0.089 w_*^2$, which amounts to a 20 percent increase in the variance at $z = z_r$.

Let us now consider some example calculations. Figures 14 and 15 show the ratio of the along-wind velocity variance predicted by the local application of Monin-Obukhov similarity to the global prediction, $\sigma_u^2 = 0.45w_*^2 + 5.8u_*^2$. The former plot is for a relatively smooth surface ($z_0/z_i = 10^{-5}$), whereas the latter is for a rough surface ($z_0/z_i = 10^{-3}$). The local theory predicts a substantial decrease of the velocity variance near the ground, particularly over a rough surface when $U_r/w_* \leq 1$. The primary cause is the previously mentioned slowdown in the velocity of the gusts when they interact with the surface.

Figures 16 and 17 show the ratio of the along-wind to the crosswind velocity variance (σ_u^2/σ_v^2), for the smooth-surface case ($z_0/z_i = 10^{-5}$). The former plot is the ratio as a function of height, whereas the latter is the ratio as a function of U_r/w_* . In highly convective conditions ($U_r/w_* \ll 1$), the turbulence structure is nearly isotropic and this ratio converges to 1. In high-wind conditions ($U_r/w_* \gg 1$), this ratio is dominated by shear turbulence and is roughly equal to $5.8/3.6 = 1.6$. Furthermore, the ratio is larger near the ground, indicating a more pronounced anisotropic structure there.

Figure 14. Ratio of along-wind velocity variance (σ_u^2) predicted by local-equilibrium model to global similarity formula $0.45 w_*^2 + 5.8 u_*^2$, for a smooth surface ($z_0/z_i = 10^{-5}$).

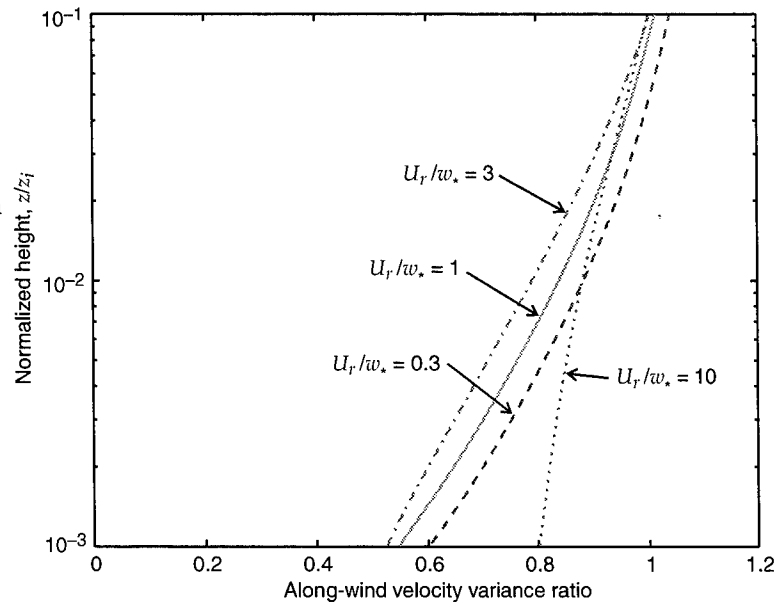


Figure 15. Same as figure 14, but for a rough surface ($z_0/z_i = 10^{-3}$).

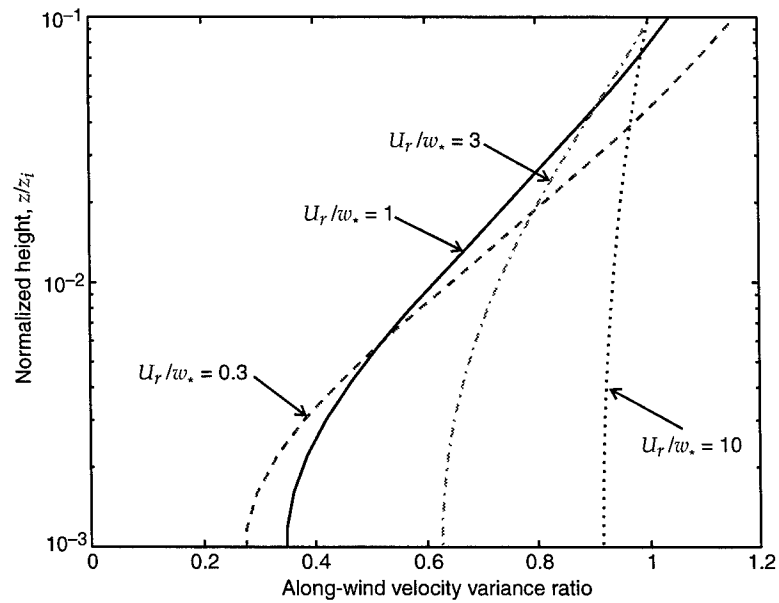


Figure 16. Ratio of along-wind to crosswind velocity variance (σ_u^2/σ_v^2) in local-equilibrium model, as a function of height, for a smooth surface ($z_0/z_i = 10^{-5}$).

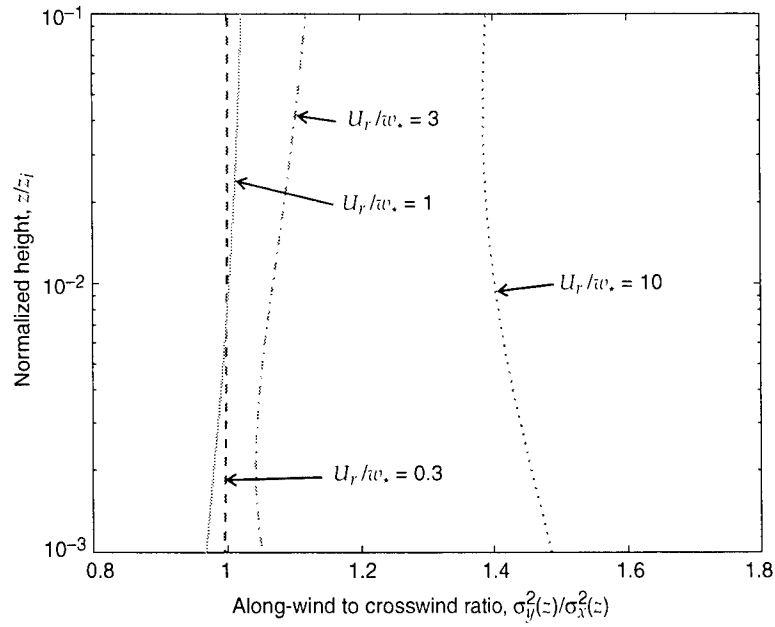
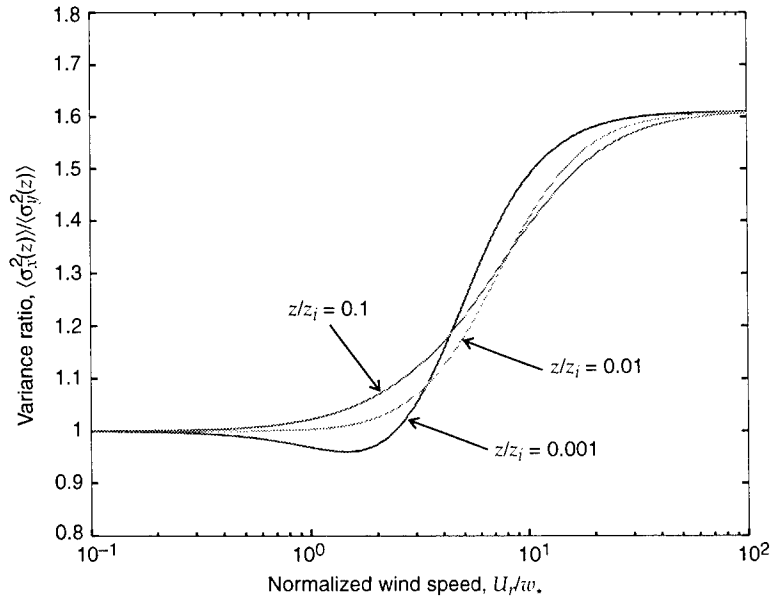


Figure 17. Ratio of along-wind to crosswind velocity variance (σ_u^2/σ_v^2) in local-equilibrium model, smooth surface case ($z_0/z_i = 10^{-5}$). Ratio versus wind speed is plotted.



At greater altitudes, the large gusts play a more prominent role, thereby diminishing the anisotropy.

Figure 17 suggests that near the ground, for moderate values of U_r/w_* , the crosswind variance may actually exceed the along-wind variance. This behavior is caused primarily by the action of gusts whose orientation runs counter to the prevailing wind direction. In the presence of such gusts, the local conditions can very closely approximate free convection. Gusts in the prevailing crosswind direction cannot cause local slackening of the wind to such a degree.

As illustrated by figures 14 through 17, the local-equilibrium model predicts behavior of the surface-layer horizontal velocity variances, which is more complex than previously thought. It would be desirable to have a simple equation that approximates the full behavior of the local equilibrium model. We discovered in deriving equations (88) and (93) that there are three contributions to the variance: global shear production by the mean wind, local shear production from the gusts, and the direct contribution from the gusts. For the along-wind variance, the global shear production contribution can be approximated as $5.8 u_*^2$. This term would naturally diminish with decreasing mean wind speed. Local shear from the gusts is important primarily when $U_r/w_* \ll 1$. Since we found in section 3.1 that the free-convection approximation works reasonably well in such situations, we can approximate this term with its value from equation (93), namely $0.89 w_*^2 (z_0/z_i)^{1/3}$. For the direct contribution from the gusts, we might try using $\langle U_L(z) \rangle$ to approximate the general shape of the profile:

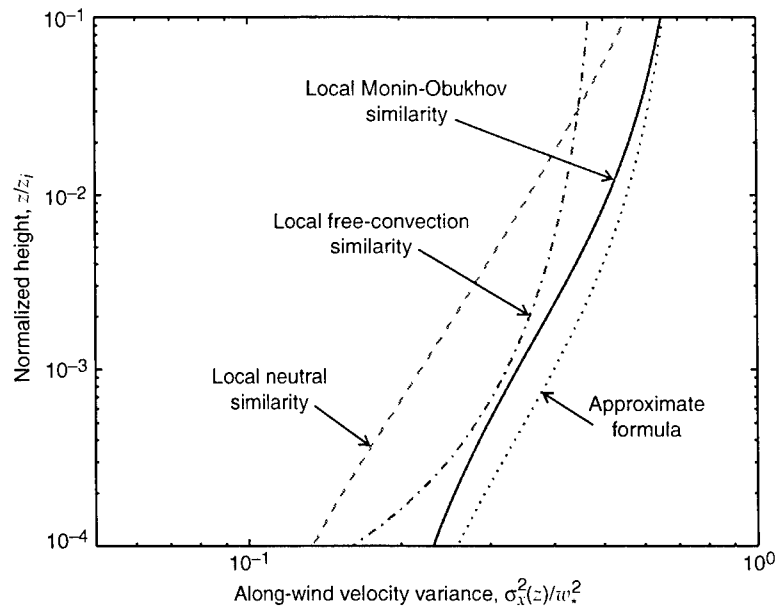
$$\langle G_x^2(z) \rangle \simeq \frac{\beta^2 w_*^2}{2} \frac{\langle U_L(z) \rangle^2}{\langle U_L(z_r) \rangle^2}. \quad (94)$$

One can show, in fact, that this equation is exact for both the local neutral and local free-convection profiles. The approximation can be applied by calculating $\langle U_L(z_r) \rangle$ from equation (12), solving equation (47) for $u_{*,\text{eff}}$, and then using this value to estimate $\langle U_L(z) \rangle$. Putting these results together yields:

$$\sigma_u^2(z) = 5.8 u_*^2 + \left\{ 0.45 \frac{\left[\frac{u_{*,\text{eff}}}{\kappa} h_M \left(\frac{z}{L_{\text{eff}}}, \frac{z_0}{L_{\text{eff}}} \right) \right]^2}{\langle U_L \rangle^2} + 0.89 \left(\frac{z_0}{z_i} \right)^{1/3} \right\} w_*^2. \quad (95)$$

An analysis of the crosswind variance results in the same formula but with 3.6 replacing 5.8 in the first term. This approximation is compared to the full local equilibrium model in figure 18 for $U_r/w_* = 0.3$ and $z_0/z_i = 10^{-5}$. Also plotted are curves based on local neutral (eq (88)) and local free-convection (eq (88)) profiles under the gusts. The approximate formula, equation (95), is quite close to the full Monin-Obukhov calculation. I have analyzed other combinations of U_r/w_* and z_0/z_i with similar satisfactory results. The effective value for u_{*L} works quite well as a shortcut to the full calculation with the pdf.

Figure 18. Local equilibrium predictions for along-wind velocity variance using several methods of calculation. For all curves, $U_r/w_* = 0.3$ and $z_0/z_i = 10^{-5}$.



4. Summary

The local-equilibrium model for gusts developed in this report suggests significant violations of widely used similarity theories, particularly when the atmosphere is very convective. For example, the inversion height (z_i) appears to affect scaling of the mean wind and temperature gradients. The primary physical reason for this behavior is that the gusts create significant local modifications to the friction velocity. On the other hand, the roughness length appears unimportant for the gradients, as had been previously concluded.

Regarding the variances, the vertical velocity variance in convective conditions is predicted to have significant dependence on both the inversion height and roughness. Near the ground, the vertical velocity variance is enhanced by local shear in the gusts. The horizontal velocity variances have a strong dependence on height and roughness, even for very moderate convection, that has not been previously recognized. The physical reason is that the wind speed in the gusts must diminish very near the surface, obtaining a roughly logarithmic height dependence. Of the variances considered in this report, only the temperature variance appears to be nearly unaffected by the gusts.

The results of this report are in qualitative agreement with the large-eddy simulations (LES) of Sykes et al (1993) and Khanna and Brasseur (1997). The former authors demonstrated a dependence of boundary-layer structure on roughness in free convection. The latter found that velocity statistics deviate significantly from Monin-Obukhov similarity, whereas temperature statistics do not. But these LES studies cannot be viewed as providing conclusive evidence in support of the local-equilibrium model: the boundary condition in LES is essentially the same as the one in the local-equilibrium model, except that it is applied between the lowermost grid level and the surface, instead of $z_r = 0.1z_i$ and the surface. Also, LES has well-documented shortcomings near the surface, because of its finite resolution. Therefore convincing verification of the predictions of the local-equilibrium model will ultimately require real atmospheric data.

Acknowledgments

This work was sponsored by an Army Research Laboratory Director's Research Initiative, "Acoustic wave propagation through characteristic ejection-sweep events in the atmospheric surface layer." Some of the ideas originate from discussions I had with J. C. Wyngaard and J. G. Brasseur during my days as a research associate at the Department of Meteorology, Pennsylvania State University, 1993 to 1995. I am indebted to them for their insights and encouragement.

Appendix A. Reference Height and Gustiness Coefficient

An important modeling issue is what value should be used for the reference height. Grachev et al (1998) used $z_r = 10$ m, because this height is a standard one for tower-based wind measurements. On the other hand, because 10 m is usually well within the surface layer, the structure of the gusts could be significantly disrupted by the ground there. Schumann (1988) based his model on a surface-layer height of $z_r = 0.1z_i$. Sykes et al (1993) took the additional step of deriving an analytical expression for z_r (z_s in their notation). However, Grachev et al (1997) subsequently demonstrated that the analysis of Sykes et al, by assuming that the local profiles under the large eddies are logarithmic, leads to implausible results.

I follow Schumann in this report by simply setting $z_r = 0.1z_i$. The main motivation for using this value instead of 10 m is that by placing the reference height in the vicinity of the top of the surface layer, the probability distribution more reasonably represents the *forcing* from the gusts rather than the *response* to them. Then the isotropic distribution, equation (8), is justifiable. Admittedly, in conditions with high mean wind shear (large U_r/w_*), the assumption of isotropy will break down even at $z_r = 0.1z_i$. However, the effect of the gusts on surface-layer statistics is negligible in such situations, since shear instability, rather than the large-scale convective eddies, will dominate the surface layer. The prescribed pdf for the gusts is at issue only for small and moderate wind speeds, for which the assumption of isotropy $z_r = 0.1z_i$ is quite reasonable.

The other model constant is the gustiness coefficient β . Previous authors have suggested several possible values. Based on their analysis of marine data at a 10-m height, Fairall et al (1996) concluded that $\beta \simeq 1.25$. Schumann (1988) determined that $\beta = 0.7 \pm 0.1$ from his model analysis. Beljaars (1994) deduced that $\beta \simeq 1.2$ from the numerical simulations of Sykes et al (1993).

A value for β can also be inferred from other sources based on the reasoning that the horizontal velocity variance for $z \geq 0.1z_i$ is determined primarily by the large-scale convective eddies. From measurements made in the lower boundary layer by aircraft, Caughey and Palmer (1979) estimated the horizontal velocity variances as $0.35w_*^2$. Since the variances $\langle G_x^2 \rangle$ and $\langle G_y^2 \rangle$ are equal to $\beta^2 w_*^2/2$, this implies that $\beta \simeq 0.84$. Similarly, Deardorff and Willis (1985) found $\sigma_{u,v}^2(z) = 0.45w_*^2$ in their laboratory experiment, which implies that $\beta \simeq 0.95$.

For the calculations in this report, I set β to 0.95, since this value falls roughly in the middle of the range of previous research results reviewed here.

Appendix B. Moments of Friction Velocity and Wind Direction

This appendix derives equations for various moments of the friction velocity and wind direction that appear in the main text. The moments have the general form $\langle u_{*L}^q \cos^m \theta \sin^n \theta \rangle$. Unfortunately, as discussed in the main text, analytical results for these moments cannot be derived when the full Monin-Obukhov form for the dimensionless wind gradient (eq (15)) is used. Therefore, in this appendix, I consider two limiting approximations for the local wind and temperature profiles, based on the limiting cases of neutral and free-convection stability.

In the neutral limit, $\Psi_M(\zeta) = 0$ and the local velocity has a logarithmic profile:

$$\mathbf{U}_L(z) = \mathbf{e}_x [\langle U(z) \rangle + G_x(z)] + \mathbf{e}_y G_y(z) = (\mathbf{e}_x \cos \theta + \mathbf{e}_y \sin \theta) \frac{u_{*L}}{\kappa} \ln \frac{z}{z_0}. \quad (\text{B-1})$$

Evaluating this equation at $z = z_r$ and taking the magnitude, one has

$$u_{*L} = \kappa \ln^{-1} \frac{z_r}{z_0} \sqrt{(U_r + G_x)^2 + G_y^2}. \quad (\text{B-2})$$

Now, substituting equations (B-2), (29), and (8) into (9) results in

$$\begin{aligned} \langle u_{*L}^q \cos^m \theta \sin^n \theta \rangle &= \frac{\kappa^q}{\pi \beta^2 w_*^2 \ln^q(z_r/z_0)} \int_{-\infty}^{\infty} \int_{-\infty}^{\infty} [(U_r + G_x)^2 + G_y^2]^{(q-m-n)/2} \\ &\quad \times (U_r + G_x)^m G_y^n \exp\left(-\frac{G_x^2 + G_y^2}{\beta^2 w_*^2}\right) dG_x dG_y. \end{aligned} \quad (\text{B-3})$$

Converting to cylindrical coordinates ρ and θ such that $\rho \cos \theta = (G_x + U_r)/\beta w_*$ and $\rho \sin \theta = G_y/\beta w_*$, the double integral becomes

$$\langle \bar{u}_{*L}^q \cos^m \theta \sin^n \theta \rangle = \frac{\kappa^q}{\pi \ln^q(z_r/z_0)} e^{-\bar{U}_r^2} \int_0^\infty \int_0^{2\pi} \rho^{q+1} \cos^m \theta \sin^n \theta \exp(-\rho^2 + 2\bar{U}_r \cos \theta) d\theta d\rho, \quad (\text{B-4})$$

where $\bar{u}_{*L} = u_{*L}/\beta w_*$ and $\bar{U}_r = U_r/\beta w_*$.

We can perform the integral over θ using the integral representation of the modified Bessel function (e.g., Abramowitz and Stegun (1965), eq (9.6.19)):

$$I_n(z) = \frac{1}{\pi} \int_0^\pi e^{z \cos \theta} \cos(n\theta) d\theta. \quad (\text{B-5})$$

Considering specific values of m and n , we therefore have

$$\langle \bar{u}_{*L}^q \rangle = \frac{2\kappa^q}{\ln^q(z_r/z_0)} e^{-\bar{U}_r^2} \int_0^\infty \rho^{q+1} e^{-\rho^2} I_0(2\bar{U}_r \rho) d\rho. \quad (\text{B-6})$$

$$\langle \bar{u}_{*L}^q \cos \theta \rangle = \frac{2\kappa^q}{\ln^q(z_r/z_0)} e^{-\bar{U}_r^2} \int_0^\infty \rho^{q+1} e^{-\rho^2} I_1(2\bar{U}_r \rho) d\rho, \quad (\text{B-7})$$

$$\langle \bar{u}_{*L}^q \cos^2 \theta \rangle = \frac{\kappa^q}{\ln^q(z_r/z_0)} e^{-\bar{U}_r^2} \int_0^\infty \rho^{q+1} e^{-\rho^2} [I_0(2\bar{U}_r \rho) + I_2(2\bar{U}_r \rho)] d\rho, \quad \text{and} \quad (\text{B-8})$$

$$\langle \bar{u}_{*L}^q \sin^2 \theta \rangle = \frac{\kappa^q}{\ln^q(z_r/z_0)} e^{-\bar{U}_r^2} \int_0^\infty \rho^{q+1} e^{-\rho^2} [I_0(2\bar{U}_r \rho) - I_2(2\bar{U}_r \rho)] d\rho. \quad (\text{B-9})$$

The latter two relationships follow from the identities $2 \cos^2 \theta = 1 + \cos 2\theta$ and $2 \sin^2 \theta = 1 - \cos 2\theta$.

The remaining integrals in equations (B-6) through (B-9) all have the form

$$\int_0^\infty t^k e^{-t^2} I_j(bt) dt.$$

The strategy for performing these integrals depends on whether $k - j$ is even or odd. When it is odd, the starting point is the following relationship, which applies to $k - j = 1$:

$$\int_0^\infty t^{\nu+1} e^{-t^2} I_\nu(bt) dt = \frac{b^\nu}{2^{\nu+1}} e^{b^2/4}. \quad (\text{B-10})$$

This relationship can be found in standard tables of integrals. For example, it is equivalent to equation (11.4.29) in Abramowitz and Stegun (1965), after applying their equation (9.6.3). The cases $k - j = 3, 5, \dots$ can be reduced to equation (B-10) by repeated applications of the recurrence formula $I_{n+1}(x) = I_{n-1}(x) - (2n/x) I_n(x)$. Solutions for even $k - j$ are based on the following result (Abramowitz and Stegun's eq (11.4.32)) for $k - j = 0$:

$$\int_0^\infty e^{-t^2} I_\nu(bt) dt = \frac{\sqrt{\pi}}{2} e^{b^2/8} I_{\nu/2}\left(\frac{b^2}{8}\right). \quad (\text{B-11})$$

The cases $k - j = 2, 4, \dots$ can be determined through integration by parts. In the formula $\int u dv = uv - \int v du$, repeatedly set $v = e^{-t^2}$ until integrals having the same form as equation (B-11) result. For reference, the special cases of interest are listed here:

$$\int_0^\infty e^{-t^2} I_0(bt) dt = \frac{\sqrt{\pi}}{2} e^{b^2/8} I_0\left(\frac{b^2}{8}\right) \quad (\text{B-12})$$

$$\int_0^\infty t^2 e^{-t^2} I_0(bt) dt = \frac{\sqrt{\pi}}{16} e^{b^2/8} \left[(4 + b^2) I_0\left(\frac{b^2}{8}\right) + b^2 I_1\left(\frac{b^2}{8}\right) \right] \quad (\text{B-13})$$

$$\int_0^\infty t^2 e^{-t^2} I_1(bt) dt = \frac{b}{4} e^{b^2/4} \quad (\text{B-14})$$

$$\int_0^\infty t^3 e^{-t^2} I_0(bt) dt = \frac{4 + b^2}{8} e^{b^2/4} \quad (\text{B-15})$$

$$\int_0^\infty t^3 e^{-t^2} I_1(bt) dt = \frac{\sqrt{\pi} b}{32} e^{b^2/8} \left[(6 + b^2) I_0\left(\frac{b^2}{8}\right) + (2 + b^2) I_1\left(\frac{b^2}{8}\right) \right] \quad (\text{B-16})$$

$$\int_0^\infty t^3 e^{-t^2} I_2(bt) dt = \frac{b^2}{8} e^{b^2/4} . \quad (\text{B-17})$$

With these integrals, we can now write down the following equations for moments of the local friction velocity:

$$\langle \bar{u}_{*L}^{-1} \rangle = \frac{\sqrt{\pi} \ln(z_r/z_0)}{\kappa} e^{-\bar{U}_r^2/2} I_0\left(\frac{\bar{U}_r^2}{2}\right) , \quad (\text{B-18})$$

$$\langle \bar{u}_{*L} \rangle = \frac{\sqrt{\pi} \kappa}{2 \ln(z_r/z_0)} e^{-\bar{U}_r^2/2} \left[(1 + \bar{U}_r^2) I_0\left(\frac{\bar{U}_r^2}{2}\right) + \bar{U}_r^2 I_1\left(\frac{\bar{U}_r^2}{2}\right) \right] , \quad (\text{B-19})$$

$$\langle \bar{u}_{*L} \cos \theta \rangle = \frac{\kappa \bar{U}_r}{\ln(z_r/z_0)} , \quad (\text{B-20})$$

$$\langle \bar{u}_{*L}^2 \cos \theta \rangle = \frac{\sqrt{\pi} \kappa^2 \bar{U}_r}{4 \ln^2(z_r/z_0)} e^{-\bar{U}_r^2/2} \left[(3 + 2\bar{U}_r^2) I_0\left(\frac{\bar{U}_r^2}{2}\right) + (1 + 2\bar{U}_r^2) I_1\left(\frac{\bar{U}_r^2}{2}\right) \right] , \quad (\text{B-21})$$

$$\langle \bar{u}_{*L}^2 \cos^2 \theta \rangle = \frac{\kappa^2}{2 \ln^2(z_r/z_0)} (1 + 2\bar{U}_r^2) , \quad \text{and} \quad (\text{B-22})$$

$$\langle \bar{u}_{*L}^2 \sin^2 \theta \rangle = \frac{\kappa^2}{2 \ln^2(z_r/z_0)} . \quad (\text{B-23})$$

Since $I_0(0) = 1$ and $I_1(0) = 0$, in the limit $\bar{U}_r \rightarrow 0$, these equations become

$$\langle \bar{u}_{*L}^{-1} \rangle = \frac{\sqrt{\pi} \ln(z_r/z_0)}{\kappa} , \quad (\text{B-24})$$

$$\langle \bar{u}_{*L} \rangle = \frac{\sqrt{\pi} \kappa}{2 \ln(z_r/z_0)} , \quad (\text{B-25})$$

$$\langle \bar{u}_{*L} \cos \theta \rangle = \langle \bar{u}_{*L}^2 \cos \theta \rangle = 0 , \quad \text{and} \quad (\text{B-26})$$

$$\langle \bar{u}_{*L}^2 \cos^2 \theta \rangle = \langle \bar{u}_{*L}^2 \sin^2 \theta \rangle = \frac{\kappa^2}{2 \ln^2(z_r/z_0)} . \quad (\text{B-27})$$

The analysis for the free-convection limit proceeds similarly to the neutral limit. Instead of equation (B-1), we use $\Psi_M(\zeta) = \ln \zeta + 3(-a_M \zeta)^{-1/3}$

(Grachev et al, 1998), resulting in

$$\begin{aligned}\mathbf{U}_L(z) &= \mathbf{e}_x [\langle U(z) \rangle + G_x(z)] + \mathbf{e}_y G_y(z) \\ &= (\mathbf{e}_x \cos \theta + \mathbf{e}_y \sin \theta) \frac{3u_{*L}^2}{\kappa^{4/3} a_M^{1/3} w_*} \left[\left(\frac{z_i}{z_0} \right)^{1/3} - \left(\frac{z_i}{z_r} \right)^{1/3} \right]\end{aligned}\quad (\text{B-28})$$

instead of equation (B-1). Evaluating this equation at $z = z_r$ and taking the magnitude, we find that

$$\langle u_{*L}^n \rangle = \left(\frac{\kappa^{4/3} a_M^{1/3} w_*}{3} \right)^{n/2} \left[\left(\frac{z_i}{z_0} \right)^{1/3} - \left(\frac{z_i}{z_r} \right)^{1/3} \right]^{-n/2} \langle G^{n/2}(z_r) \rangle. \quad (\text{B-29})$$

Therefore

$$\langle \bar{u}_{*L}^q \cos^m \theta \sin^n \theta \rangle = \frac{1}{\pi} \left(\frac{\kappa^{4/3} a_M^{1/3}}{3\beta} \right)^{q/2} \left[\left(\frac{z_i}{z_0} \right)^{1/3} - \left(\frac{z_i}{z_r} \right)^{1/3} \right]^{-q/2} e^{-\bar{U}_r^2} \quad (\text{B-30})$$

$$\times \int_0^\infty \int_0^{2\pi} \rho^{q/2+1} \cos^m \theta \sin^n \theta \exp(-\rho^2 + 2\bar{U}_r \cos \theta) d\theta d\rho. \quad (\text{B-31})$$

The integral over θ proceeds in the same manner as the neutral limit. When q is even, we can also determine the remaining integral over ρ using the previous methodology. Integration for odd q leads to confluent hypergeometric functions. However, since the free-convection limit should be useful only for small \bar{U}_r , we may simplify the integrations by setting $\bar{U}_r = 0$. With this approximation,

$$\langle \bar{u}_{*L}^q \cos^m \theta \sin^n \theta \rangle \simeq \frac{1}{\pi} \left(\frac{\kappa^{4/3} a_M^{1/3}}{3\beta} \right)^{q/2} \left[\left(\frac{z_i}{z_0} \right)^{1/3} - \left(\frac{z_i}{z_r} \right)^{1/3} \right]^{-q/2} \quad (\text{B-32})$$

$$\times \int_0^\infty \int_0^{2\pi} \rho^{q/2+1} \cos^m \theta \sin^n \theta \exp(-\rho^2) d\theta d\rho. \quad (\text{B-33})$$

The integrations now yield

$$\langle \bar{u}_{*L}^q \rangle = \Gamma(q/4 + 1) \left(\frac{\kappa^{4/3} a_M^{1/3}}{3\beta} \right)^{q/2} \left[\left(\frac{z_i}{z_0} \right)^{1/3} - \left(\frac{z_i}{z_r} \right)^{1/3} \right]^{-q/2}, \quad (\text{B-34})$$

$$\langle \bar{u}_{*L}^q \cos \theta \rangle = 0, \quad (\text{B-35})$$

$$\langle \bar{u}_{*L}^q \cos^2 \theta \rangle = \langle \bar{u}_{*L}^q \sin^2 \theta \rangle = \frac{\Gamma(q/4 + 1)}{2} \left(\frac{\kappa^{4/3} a_M^{1/3}}{3\beta} \right)^{q/2} \left[\left(\frac{z_i}{z_0} \right)^{1/3} - \left(\frac{z_i}{z_r} \right)^{1/3} \right]^{-q/2}, \quad (\text{B-36})$$

and

$$\langle \bar{u}_{*L}^q \sin^2 \theta \rangle = \frac{\Gamma(q/4 + 1)}{2} \left(\frac{\kappa^{4/3} a_M^{1/3}}{3\beta} \right)^{q/2} \left[\left(\frac{z_i}{z_0} \right)^{1/3} - \left(\frac{z_i}{z_r} \right)^{1/3} \right]^{-q/2}. \quad (\text{B-37})$$

Figures B-1 and B-2 compare the neutral and free-convection limits to full Monin-Obukhov similarity for moments involving \bar{u}_{*L} and $\cos \theta$. The plots show that neither the neutral nor the free-convection limits provide a very satisfactory approximation. As \bar{U}_r increases, the neutral limit prediction converges very slowly to full Monin-Obukhov similarity, differing by more than 10 percent even at $\bar{U}_r = 10$. The free-convection prediction very roughly approximates (to within about 30%) the moments $\langle \bar{u}_{*L} \rangle$ and $\langle \bar{u}_{*L}^2 \cos^2 \theta \rangle$ when $\bar{U}_r \ll 1$.

Figure B-1. Statistical moments $\langle \bar{u}_{*L} \rangle$ and $\langle \bar{u}_{*L} \cos \theta \rangle$ as a function of normalized wind speed \bar{U}_r . Local equilibrium predictions that use full Monin-Obukhov similarity, as well as approximate predictions in neutral and free-convection limits, are shown. Roughness length is $10^{-5} z_i$. (Free-convection prediction for $\langle \bar{u}_{*L} \cos \theta \rangle$ is zero.)

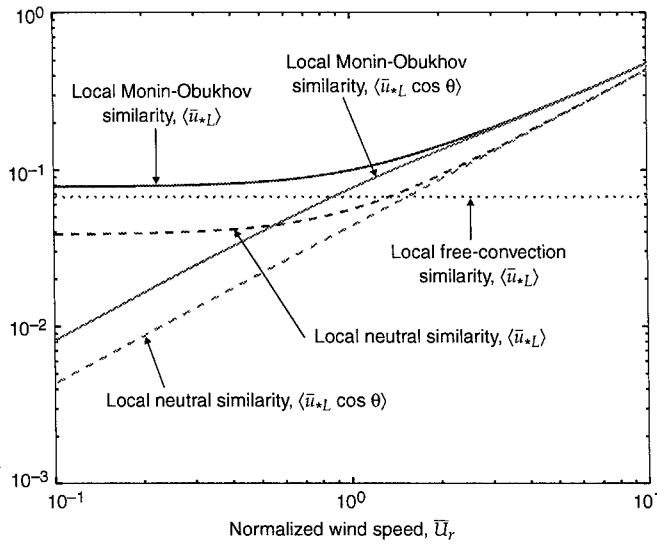
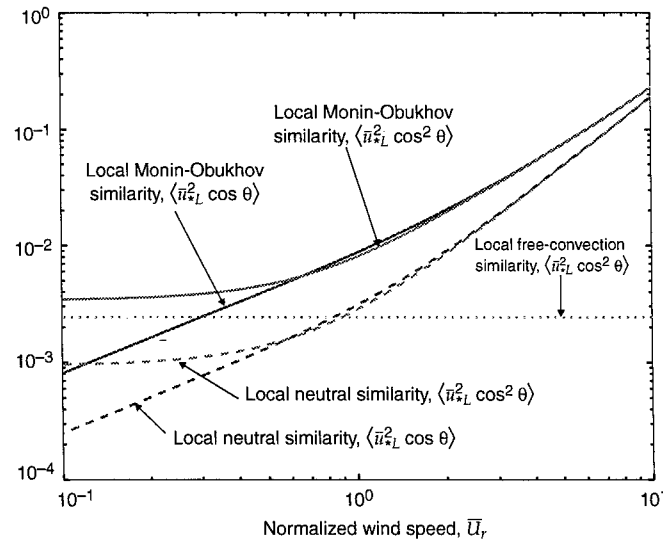


Figure B-2. Same as figure B-1, except for statistical moments $\langle \bar{u}_{*L} \cos^2 \theta \rangle$ and $\langle \bar{u}_{*L}^2 \cos^2 \theta \rangle$. (Free-convection prediction for $\langle \bar{u}_{*L} \cos^2 \theta \rangle$ is zero.)



References

- Abramowitz, M., and I. A. Stegun (1965): *Handbook of Mathematical Functions*. Dover, San Francisco.
- Batchelor, G. K. (1953): *The Theory of Homogeneous Turbulence*. Cambridge Univ. Press, Cambridge, Great Britain.
- Beljaars, A.C.M. (1994): The parameterization of surface fluxes in large-scale models under free convection. *Q. J. R. Meteorol. Soc.* **121**, 255–270.
- Businger, J. A. (1973a): A note on free convection. *Boundary-Layer Meteorol.* **4**, 323–326.
- Businger, J. A. (1973b): Turbulent transfer in the atmospheric surface layer. In *Workshop on Micrometeorology*, Haugen, D. A., ed., American Meteorological Society, Boston, 67–100.
- Businger, J. A., J. C. Wyngaard, Y. Izumi, and E. F. Bradley (1971): Flux-profile relationships in the atmospheric surface layer. *J. Atmos. Sci.* **28**, 181–189.
- Carl, D. M., T. C. Tarbell, and H. A. Panofsky (1973): Profiles of wind and temperature from towers over homogeneous terrain. *J. Atmos. Sci.* **30**, 181–189.
- Caughey, S. J., and S. G. Palmer (1979): Some aspects of turbulence structure through the depth of the convective boundary layer. *Q. J. R. Meteorol. Soc.* **105**, 811–827.
- Deardorff, J. W. (1970): Convective velocity and temperature scales for the unstable planetary boundary layer and for raleigh convection. *J. Atmos. Sci.* **27**, 1211–1213.
- Deardorff, J. W., and G. E. Willis (1985): Further results from a laboratory model of the convective planetary boundary layer. *Boundary-Layer Meteorol.* **32**, 205–236.
- Fairall, C. W., E. F. Bradley, D. P. Rogers, J. B. Edson, and G. S. Young (1996): Air-sea flux parameterization in TOGA COARE. *J. Geophys. Res.* **101(C2)**, 3747–3764.
- Garratt, J. R. (1992): *The Atmospheric Boundary Layer*. Cambridge University Press, Cambridge, Great Britain.
- Godfrey, J. S., and A.C.M. Beljaars (1991): On the turbulent fluxes of buoyancy, heat, and moisture at the air-sea interface at low wind speeds. *J. Geophys. Res.* **96**, 22,043–22,048.

- Grachev, A. A., C. W. Fairall, and S. E. Larsen (1998): On the determination of the neutral drag coefficient in the convective boundary layer. *Boundary-Layer Meteorol.* **86**, 257–278.
- Grachev, A. A., C. W. Fairall, and S. S. Zilitinkevich (1997): Surface-layer scaling for the convection-induced stress regime. *Boundary-Layer Meteorol.* **83**, 423–439.
- Högström, U. (1988): Non-dimensional wind and temperature profiles in the atmospheric surface layer. *Boundary-Layer Meteorol.* **42**, 263–270.
- Højstrup, J. (1982): Velocity spectra in the unstable planetary boundary layer. *J. Atmos. Sci.* **39**, 2239–2248.
- Kader, B. A., and A. M. Yaglom (1990): Mean fields and fluctuation moments in unstably stratified turbulent boundary layers. *J. Fluid Mech.* **212**, 637–662.
- Kaimal, J. C., J. C. Wyngaard, D. A. Haugen, O. R. Coté, and Y. Izumi (1976): Turbulence structure in the convective boundary layer. *J. Atmos. Sci.* **33**, 2152–2169.
- Khanna, S., and J. G. Brasseur (1997): Analysis of Monin-Obukhov similarity from large-eddy simulations. *J. Fluid Mech.* **345**, 251–286.
- Kraichnan, R. H. (1962): Turbulent thermal convection at arbitrary Prandtl number. *Phys. Fluids* **5**, 1374–1389.
- Monin, A. S., and A. M. Obukhov (1954): Basic laws of turbulent mixing in the atmosphere near the ground. *Tr. Akad. Nauk SSR Geofiz. Inst.* **24**, 163–187.
- Panofsky, H. A., and J. A. Dutton (1984): *Atmospheric Turbulence: Models and Methods for Engineering Applications*. John Wiley & Sons, New York.
- Panofsky, H. A., H. Tennekes, D. H. Lenschow, and J. C. Wyngaard (1977): The characteristics of turbulent velocity components in the surface layer under convective conditions. *Boundary-Layer Meteorol.* **11**, 355–361.
- Peltier, L. J., J. C. Wyngaard, S. Khanna, and J. G. Brasseur (1996): Spectra in the unstable surface layer. *J. Atmos. Sci.* **53**, 49–61.
- Schumann, U. (1988): Minimum friction velocity and heat transfer in the rough surface layer of a convective boundary layer. *Boundary-Layer Meteorol.* **44**, 311–326.
- Stull, R. B. (1988): *An Introduction to Boundary Layer Meteorology*. Kluwer, Dordrecht, Germany.
- Sykes, R. I., D. S. Henn, and W. S. Lewellen (1993): Surface-layer description under free-convection conditions. *Q. J. R. Meteorol. Soc.* **119**, 409–421.
- Tennekes, H., and J. L. Lumley (1972): *A First Course in Turbulence*. MIT Press, Cambridge, Massachusetts.

- Tong, C. N., J. C. Wyngaard, S. Khanna, and J. G. Brasseur (1998): Resolvable- and subgrid-scale measurement in the atmospheric surface layer: Techniques and issues. *J. Atmos. Sci.* **55**, 3114–3126.
- Wilson, D. K., and D. W. Thomson (1994): Acoustic propagation through anisotropic, surface-layer turbulence. *J. Acoust. Soc. Am.* **96**, 1080–1095.
- Wyngaard, J. C., O. R. Coté, and Y. Izumi (1971): Local free convection, similarity, and the budgets of shear stress and heat flux. *J. Atmos. Sci.* **28**, 1171–1182.

Distribution

Admnstr
Defns Techl Info Ctr
ATTN DTIC-OCF
8725 John J Kingman Rd Ste 0944
FT Belvoir VA 22060-6218

DARPA
ATTN S Welby
3701 N Fairfax Dr
Arlington VA 22203-1714

Mil Asst for Env Sci
Ofc of the Undersec of Defns for Rsrch &
Engrg R&AT E LS
Pentagon Rm 3D129
Washington DC 20301-3080

Ofc of the Secy of Defns
ATTN ODDRE (R&AT)
The Pentagon
Washington DC 20301-3080

Ofc of the Secy of Defns
ATTN OUSD(A&T)/ODDR&E(R) R J Trew
3080 Defense Pentagon
Washington DC 20301-7100

AMCOM MRDEC
ATTN AMSMI-RD W C McCorkle
Redstone Arsenal AL 35898-5240

US Army Corps of Engrs Engr
Topographics Lab
ATTN CETEC-TR-G P F Krause
7701 Telegraph Rd
Alexandria VA 22315-3864

US Army Field Artillery Schl
ATTN ATSF-TSM-TA
FT Sill OK 73503-5000

US Army Infantry
ATTN ATSH-CD-CS-OR E Dutoit
FT Benning GA 30905-5090

US Army Materiel Sys Anal Actvty
ATTN AMXSY-CS Bradley
Aberdeen Proving Ground MD 21005-5071

US Army TACOM-ARDEC
ATTN AMSTA-AR-WEL-TL
Bldg 59 Phillips Rd
Picatinny Arsenal NJ 07806-5000

Dir for MANPRINT
Ofc of the Deputy Chief of Staff for Prsnl
ATTN J Hiller
The Pentagon Rm 2C733
Washington DC 20301-0300

Natl Ground Intllgnc Ctr
Army Foreign Sci Tech Ctr
ATTN CM
220 7th Stret NE
Charlottesville VA 22901-5396

Natl Security Agcy
ATTN W21 Longbothum
9800 Savage Rd
FT George G Meade MD 20755-6000

SMC/CZA
2435 Vela Way Ste 1613
El Segundo CA 90245-5500

TECOM
ATTN AMSTE-CL
Aberdeen Proving Ground MD 21005-5057

US Army ARDEC
ATTN AMSTA-AR-TD
Picatinny Arsenal NJ 07806-5000

US Army CRREL
ATTN CRREL-GP R Detsch
72 Lyme Rd
Hanover NH 03755-1290

US Army Dugway Proving Ground
ATTN STEDP 3
ATTN STEDP-MT-DA-L-3
ATTN STEDP-MT-M Bowers
Dugway UT 84022-5000

US Army Info Sys Engrg Cmnd
ATTN AMSEL-IE-TD F Jenia
FT Huachuca AZ 85613-5300

Distribution (cont'd)

US Army Natick RDEC
Acting Techl Dir
ATTN SBCN-T P Brandler
Natick MA 01760-5002

US Army OEC
ATTN CSTE-AEC-FSE
4501 Ford Ave Park Center IV
Alexandria VA 22302-1458

US Army Simulation Train & Instrmntn
Cmnd
ATTN AMSTI-CG M Macedonia
ATTN J Stahl
12350 Research Parkway
Orlando FL 32826-3726

US Army Soldier & Biol Chem Cmnd
Dir of Rsrch & Techlgy Dirctr
ATTN SMCCR-RS IG Resnick
Aberdeen Proving Ground MD 21010-5423

US Army Tank-Automtv Cmnd RDEC
ATTN AMSTA-TR J Chapin
Warren MI 48397-5000

US Army TRADOC Anal Cmnd—WSMR
ATTN ATRC-WSS-R
White Sands Missile Range NM 88002

US Army TRADOC
Battle Lab Integration & Techl Dirctr
ATTN ATCD-B
ATTN ATCD-B J A Klevecz
FT Monroe VA 23651-5850

US Military Acdmy
Mathematical Sci Ctr of Excellence
ATTN MADN-MATH MAJ M Huber
Thayer Hall
West Point NY 10996-1786

USATRADOC
ATTN ATCD-FA
FT Monroe VA 23651-5170

Nav Air War Cen Wpn Div
ATTN CMD 420000D C0245 A Shlanta
1 Admin Cir
China Lake CA 93555-6001

Nav Surfc Warfare Ctr
ATTN Code B07 J Pennella
17320 Dahlgren Rd Bldg 1470 Rm 1101
Dahlgren VA 22448-5100

Naval Surfc Weapons Ctr
ATTN Code G63
Dahlgren VA 22448-5000

AFCCC/DOC
ATTN Glauber
151 Patton Ave Rm 120
Asheville NC 28801-5002

Hdqtrs AFWA/DNX
106 Peacekeeper Dr Ste 2N3
Offutt AFB NE 68113-4039

USAF Rome Lab Tech
ATTN Corridor W Ste 262 RL SUL
26 Electr Pkwy Bldg 106
Griffiss AFB NY 13441-4514

Hicks & Assoc Inc
ATTN G Singley III
1710 Goodrich Dr Ste 1300
McLean VA 22102

Director
US Army Rsrch Ofc
ATTN AMSRL-RO-D JCI Chang
ATTN AMSRL-RO-EN W D Bach
PO Box 12211
Research Triangle Park NC 27709

US Army Rsrch Lab
ATTN AMSRL-D D R Smith
ATTN AMSRL-DD J M Miller
ATTN AMSRL-CI-AI-R Mail & Records
Mgmt
ATTN AMSRL-CI-AP Techl Pub (3 copies)
ATTN AMSRL-CI-LL Techl Lib (3 copies)
ATTN AMSRL-CI-EM D Garvey
ATTN AMSRL-CI-EM J Mercurio
ATTN AMSRL-CI-EM S Chang
ATTN AMSRL-CI-EP D K Wilson (8 copies)
Adelphi MD 20783-1197

REPORT DOCUMENTATION PAGE			Form Approved OMB No. 0704-0188	
Public reporting burden for this collection of information is estimated to average 1 hour per response, including the time for reviewing instructions, searching existing data sources, gathering and maintaining the data needed, and completing and reviewing the collection of information. Send comments regarding this burden estimate or any other aspect of this collection of information, including suggestions for reducing this burden, to Washington Headquarters Services, Directorate for Information Operations and Reports, 1215 Jefferson Davis Highway, Suite 1204, Arlington, VA 22202-4302, and to the Office of Management and Budget, Paperwork Reduction Project (0704-0188), Washington, DC 20503.				
1. AGENCY USE ONLY (Leave blank)		2. REPORT DATE December 2000		3. REPORT TYPE AND DATES COVERED Final, Apr 1998-Feb 2000
4. TITLE AND SUBTITLE The Role of Wind Gusts in the Near-Ground Atmosphere			5. FUNDING NUMBERS DA PR: B53A PE: 61102A	
6. AUTHOR(S) D. Keith Wilson				
7. PERFORMING ORGANIZATION NAME(S) AND ADDRESS(ES) U.S. Army Research Laboratory Attn: AMSRL-CI-EP email: dkwilson@arl.army.mil 2800 Powder Mill Road Adelphi, MD 20783-1197			8. PERFORMING ORGANIZATION REPORT NUMBER ARL-TR-2290	
9. SPONSORING/MONITORING AGENCY NAME(S) AND ADDRESS(ES) U.S. Army Research Laboratory 2800 Powder Mill Road Adelphi, MD 20783-1197			10. SPONSORING/MONITORING AGENCY REPORT NUMBER	
11. SUPPLEMENTARY NOTES ARL PR: 0FEJ60 AMS code: 61110253A11				
12a. DISTRIBUTION/AVAILABILITY STATEMENT Approved for public release; distribution unlimited.			12b. DISTRIBUTION CODE	
13. ABSTRACT (Maximum 200 words) Gusts from boundary-layer-scale convective eddies modify the structure of the atmospheric surface layer by intermittently intensifying or diminishing the local wind speed. A simple model for the effects of these gusts is proposed, based on the following two assumptions: (1) the wind gusts have an isotropic Gaussian probability distribution with standard deviation proportional to w_* (the convective velocity scale) and (2) the surface-layer wind and temperature profiles attain local equilibrium with the wind gusts. The minimum friction velocity predicted by the model has the same dependence on surface roughness predicted by Schumann's earlier "slab" model for convective boundary layers. However, the current model also applies to situations where the mean wind is nonzero. It predicts the breakdown of global Monin-Obukhov similarity for the surface-layer windshear and temperature gradient in highly convective conditions (U_r/w_* approximately 1 or smaller, where U_r is the mean wind speed at the top of the surface layer). Also in contrast to existing similarity theories, the horizontal wind variance exhibits a significant dependence on height and surface roughness near the ground, even for moderate convection. The temperature variance is nearly unaffected by the gusts, because of its weak dependence on the local wind speed in convective conditions.				
14. SUBJECT TERMS Turbulence, boundary-layer thermals, Monin-Obukhov similarity			15. NUMBER OF PAGES 54	
			16. PRICE CODE	
17. SECURITY CLASSIFICATION OF REPORT Unclassified	18. SECURITY CLASSIFICATION OF THIS PAGE Unclassified	19. SECURITY CLASSIFICATION OF ABSTRACT Unclassified	20. LIMITATION OF ABSTRACT UL	